Cell

Article

Mouse oocytes sequester aggregated proteins in degradative super-organelles

Graphical abstract

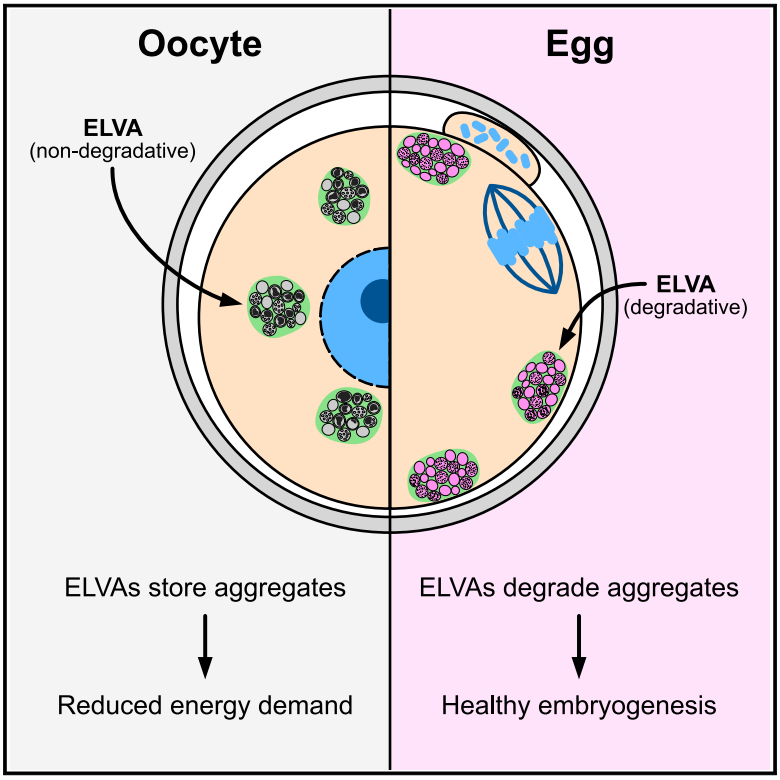

Authors

Gabriele Zaffagnini, Shiya Cheng, Marion C. Salzer, ..., Manuel Irimia, Melina Schuh, Elvan Böke

Correspondence

elvan.boke@crg.eu

In brief

Mouse oocytes store protein aggregates in liquid-like compartments that we named endolysosomal vesicular assemblies (ELVAs) in which the aggregates are degraded upon oocyte maturation. Failure to degrade aggregates in ELVAs causes early embryonic arrest.

Highlights

- Mouse oocytes store protein aggregates in endolysosomal vesicular assemblies (ELVAs)
- ELVAs harbor endolysosomes, autophagosomes, and proteasomes in a liquid-like matrix
- ELVAs degrade aggregates upon oocyte maturation to promote healthy embryogenesis
- Retention of protein aggregates in the embryo leads to early embryonic arrest

Zaffagnini et al., 2024, Cell *187*, 1109–1126
February 29, 2024
https://doi.org/10.1016/j.cell.2024.01.031

CellPress

Cell

CellPress
OPEN ACCESS

Article

Mouse oocytes sequester aggregated proteins in degradative super-organelles

Gabriele Zaffagnini,[1] Shiya Cheng,[2] Marion C. Salzer,[1] Barbara Pernaute,[1,6] Juan Manuel Duran,[1] Manuel Irimia,[1,3,4] Melina Schuh,[2,5] and Elvan Böke[1,3,7,*]

[1]Centre for Genomic Regulation (CRG), The Barcelona Institute of Science and Technology, Dr. Aiguader 88, 08003 Barcelona, Spain
[2]Department of Meiosis, Max Planck Institute for Multidisciplinary Sciences, 37077 Göttingen, Germany
[3]Universitat Pompeu Fabra (UPF), Barcelona, Spain
[4]ICREA, Pg. Lluís Companys 23, 08010 Barcelona, Spain
[5]Cluster of Excellence "Multiscale Bioimaging: from Molecular Machines to Networks of Excitable Cells" (MBExC), University of Göttingen, 37077 Göttingen, Germany
[6]Present address: Centro Andaluz de Biología del Desarrollo (CABD-CSIC), Ctra. Utrera Km. 1, 41013 Sevilla, Spain
[7]Lead contact
*Correspondence: elvan.boke@crg.eu
https://doi.org/10.1016/j.cell.2024.01.031

SUMMARY

Oocytes are among the longest-lived cells in the body and need to preserve their cytoplasm to support proper embryonic development. Protein aggregation is a major threat for intracellular homeostasis in long-lived cells. How oocytes cope with protein aggregation during their extended life is unknown. Here, we find that mouse oocytes accumulate protein aggregates in specialized compartments that we named endolysosomal vesicular assemblies (ELVAs). Combining live-cell imaging, electron microscopy, and proteomics, we found that ELVAs are non-membrane-bound compartments composed of endolysosomes, autophagosomes, and proteasomes held together by a protein matrix formed by RUFY1. Functional assays revealed that in immature oocytes, ELVAs sequester aggregated proteins, including TDP-43, and degrade them upon oocyte maturation. Inhibiting degradative activity in ELVAs leads to the accumulation of protein aggregates in the embryo and is detrimental for embryo survival. Thus, ELVAs represent a strategy to safeguard protein homeostasis in long-lived cells.

INTRODUCTION

Oocytes are the female germ cells. In most mammals, oocytes are formed during fetal development and survive decades before being employed for reproduction. Upon maturation and ovulation, oocytes become fertilizable eggs, which provide virtually all the cytoplasm to the new embryo. Therefore, the mature oocyte must ensure passing damage-free cytoplasm to the embryo to preserve its developmental potential.[1]

Protein degradation is essential for maintaining a healthy cytoplasm, as failure to remove misfolded or damaged proteins from the cell leads to the accumulation of toxic protein aggregates. Two highly interconnected proteolytic systems, the ubiquitin-proteasome system and the autophagy-lysosomal pathway, are central for protein degradation.[2] While soluble ubiquitinated polypeptides are targeted to the ubiquitin-proteasome system, insoluble aggregates of ubiquitinated proteins are typically degraded via the autophagy-lysosomal pathway.[2,3] Autophagy is essential for early embryonic development[4] and the maintenance of ovarian reserve in mice.[5] It is also implicated in oocyte maturation[6] and death[7] in some species. Proteasomal degradation is essential for meiotic maturation.[8] How the activities of these two systems are regulated during oocyte growth and maturation is not well known.

Long-lived, non-dividing cells such as oocytes and neurons are particularly sensitive to the accumulation of protein aggregates, as these cells cannot dissipate aggregates by cell division.[9] Although the formation, accumulation, and physiological clearance mechanisms of protein aggregates in neurons are intensely studied,[10] how long-lived mammalian oocytes cope with protein aggregation is unknown.[11]

RESULTS

Mouse oocytes sequester protein aggregates in non-membrane-bound compartments

To investigate whether mammalian oocytes contain protein aggregates, we isolated oocytes, eggs, and early embryos from young adult mice (up to 12 weeks old) and probed them with Proteostat, a dye that has been widely used to monitor protein aggregation[12–14] (Figure 1A). We found that all freshly isolated oocytes and eggs contain large μm-sized Proteostat-positive compartments, indicative of the existence of aggregates in these cells (Figures 1A–1E and S1A). The *in vitro* maturation and

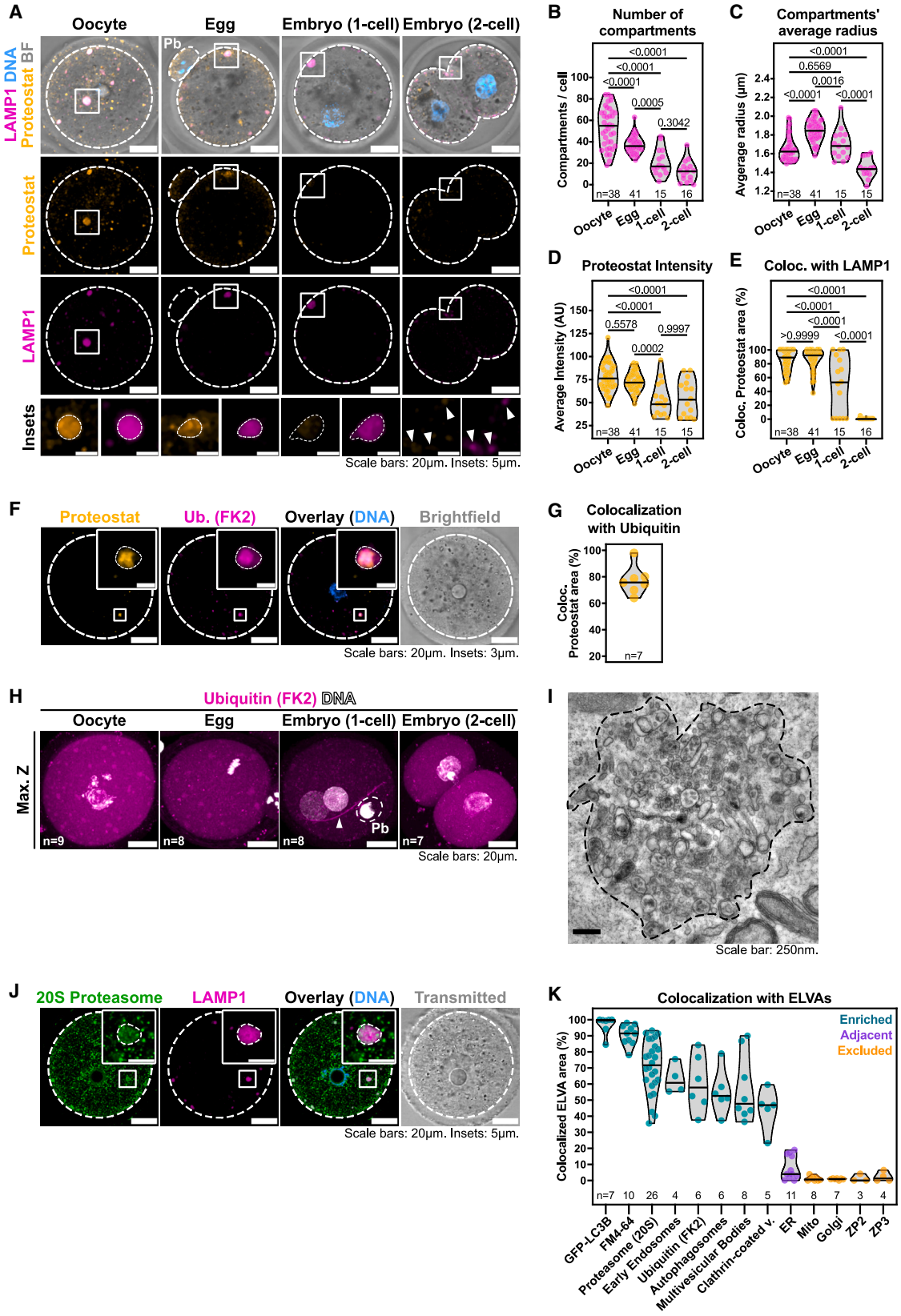

(legend on next page)

blastocyst formation rates of these oocytes and embryos were 70.2% (n = 1,811) and 71.8% (n = 86), respectively, in line with other reports in the literature, confirming their viability.[15,16] Proteostat-positive compartments disappeared during the first embryonic cleavage, suggesting that aggregates are cleared following fertilization (Figures 1A–1E and S1A).

We next asked whether the Proteostat-positive compartments in oocytes would be characterized by the accumulation of ubiquitin and would colocalize with lysosomes. Indeed, they were labeled by the late endosomal/lysosomal marker LAMP1 (lysosome-associated membrane glycoprotein 1) and by a monoclonal antibody against ubiquitinated substrates (FK2) in all oocytes (Figures 1A–1H and S1A). These Proteostat- and LAMP1-positive compartments were also visible in mouse ovarian sections, confirming their presence *in vivo* (Figures S1B and S1C). Moreover, all oocytes isolated from the ovaries of two other mouse strains, the outbred CD1 and the inbred FvB/N, also contained Proteostat-positive large compartments that colocalized with LAMP1 (Figures S1D and S1E), indicating that these compartments are present in ovaries of mice with different genetic backgrounds. Together, these data show that mouse oocytes contain large ubiquitinated protein aggregates, which disappear during early embryonic development (Figures 1A, 1H, and S1A).

LAMP1 is a transmembrane protein, and its filled-sphere-like immunofluorescence pattern in oocytes (Figures 1A, S1A, S1B, and S1D) suggested that the compartments we identified are an accumulation of several lysosomes and possibly other organelles, as opposed to a large vacuole or lysosome. To characterize these compartments further, we examined their ultrastructure by immunocorrelative light and electron microscopy (immuno-CLEM) as well as electron tomography (ET) (Figures 1I and S1F; Video S1). LAMP1 assemblies appeared in immuno-CLEM and ET as non-membrane-bound clusters of endolysosomal and autophagy vesicles, including early endosomes, late endosomes/multivesicular bodies (MVBs), autophagosomes, and autolysosomes (Figures 1I and S1F; Video S1).[18] We also observed that the clusters contained clathrin-coated vesicles and were occasionally in contact with endoplasmic reticulum (ER) tubules but appeared devoid of mitochondria and Golgi cisternae (Figures 1I and S1F; Video S1). We confirmed these results by assessing the colocalization of Proteostat and LAMP1 with markers for each of these organelles (Figures 1K and S1G–S1J). Consistent with the lack of Golgi cisternae inside the compartments, we did not observe secreted cargos, such as Zona Pellucida proteins, colocalizing with them (Figures 1K and S1K). Similar clusters of vesicles in mammalian oocytes were previously referred to as "multivesicular aggregates," "multivesicular complexes," or "multivesicular bodies" in descriptive electron microscopy studies.[19–22] To avoid confusion with actual MVBs, one of the vesicle types found inside the compartments, and to highlight their selective endolysosomal composition, we renamed these compartments endolysosomal vesicular assemblies (ELVAs). ELVAs also contain proteasomes, as evidenced by their colocalization with the core Proteasome particle (20S) (Figures 1J, 1K, S1I, and S1J).

We concluded that ELVAs are non-membrane-bound compartments that host several membranous organelles, and thus we refer to them as "super-organelles." ELVAs sequester ubiquitinated protein aggregates in oocytes and host both the major intracellular protein degradation pathways, namely the ubiquitin-proteasome system and the autophagy-lysosomal pathway.

ELVAs relocate to the cortex during oocyte maturation in an actin-dependent manner

We hypothesized that ELVAs should be distributed throughout the oocyte cytoplasm to sequester aggregated proteins in immature oocytes. To probe the distribution of ELVAs, we developed a macro to identify ELVAs from 3D sections (Figures S2A–S2C) and quantified the distance of individual ELVAs from the cell cortex (Figures 2A and 2B). We found that ELVAs were distributed in the cytoplasm of maturation-incompetent (NSN) and -competent (SN) oocytes (Figures 2A and 2B). Interestingly, ELVAs were adjacent to the cortex in eggs and 1-cell embryos, suggesting that they relocate during oocyte maturation (Figures 2A and 2B). We further observed that the ELVA number per oocyte decreased from surrounded nucleolus (SN) oocytes to eggs, whereas ELVA size increased, suggesting that ELVAs may fuse with each other during oocyte maturation (Figures 1B, 1C, 2C, and 2D). To follow ELVA movements directly, we labeled ELVAs in live oocytes with the endocytic probe FM4-64FX (Figures 1K and S2D) and followed them with 4D-microscopy during oocyte maturation (Figures 2E and 2F; Video S2).

Figure 1. Mouse oocytes contain protein aggregates that are degraded during embryonic development

(A) Confocal images of isolated mouse C57BL/6J oocytes, eggs, and early embryos labeled with Proteostat and an antibody against the lysosome marker LAMP1. In addition to the LAMP1-positive compartments, in eggs, Proteostat also labels the degenerated polar body (Pb).[17]

(B–E) Quantification of the number (B), average radius (C), mean Proteostat intensity (D), and colocalization with LAMP1 (E) of the Proteostat compartments shown in (A). In all figures, data points depict the mean values per cell (average of all the compartments measured per cell), and n indicates the number of individual cells analyzed per condition isolated from multiple animals. p values: one-way ANOVA with Šidák correction for multiple comparisons.

(F) Confocal images of a representative .mouse oocyte labeled with Proteostat and anti-ubiquitin conjugates (FK2).

(G) Colocalization of ubiquitin and Proteostat in the experiment shown in (F).

(H) Confocal maximal Z projections of mouse oocyte, egg, and 1- and 2-cell embryos immunolabeled with anti-ubiquitin conjugates (FK2). Arrowhead: sperm tail. Pb, polar body.

(I) Electron micrograph of a Proteostat-LAMP1 positive compartment (ELVA). The dashed line indicates the ELVA boundary.

(J) Confocal image of a mouse oocyte immunolabeled with anti-LAMP1 and anti-proteasome 20S.

(K) Colocalization of the indicated proteins/dyes/organelles with ELVAs. ELVAs were labeled with anti-LAMP1, early endosomes with anti-EEA1, autophagosomes with anti-LC3B, multivesicular bodies with anti-HGS, Clathrin-coated vesicles with anti-Clathrin light chain (CLTC), ER with anti-calnexin (CANX), mitochondria (Mito) with anti-citrate synthase (CS), and Golgi with anti-GM130. Representative images of each sample are shown in Figures 1J, S1G, S1H, S1K, S2D, and 3A.

See also Figure S1.

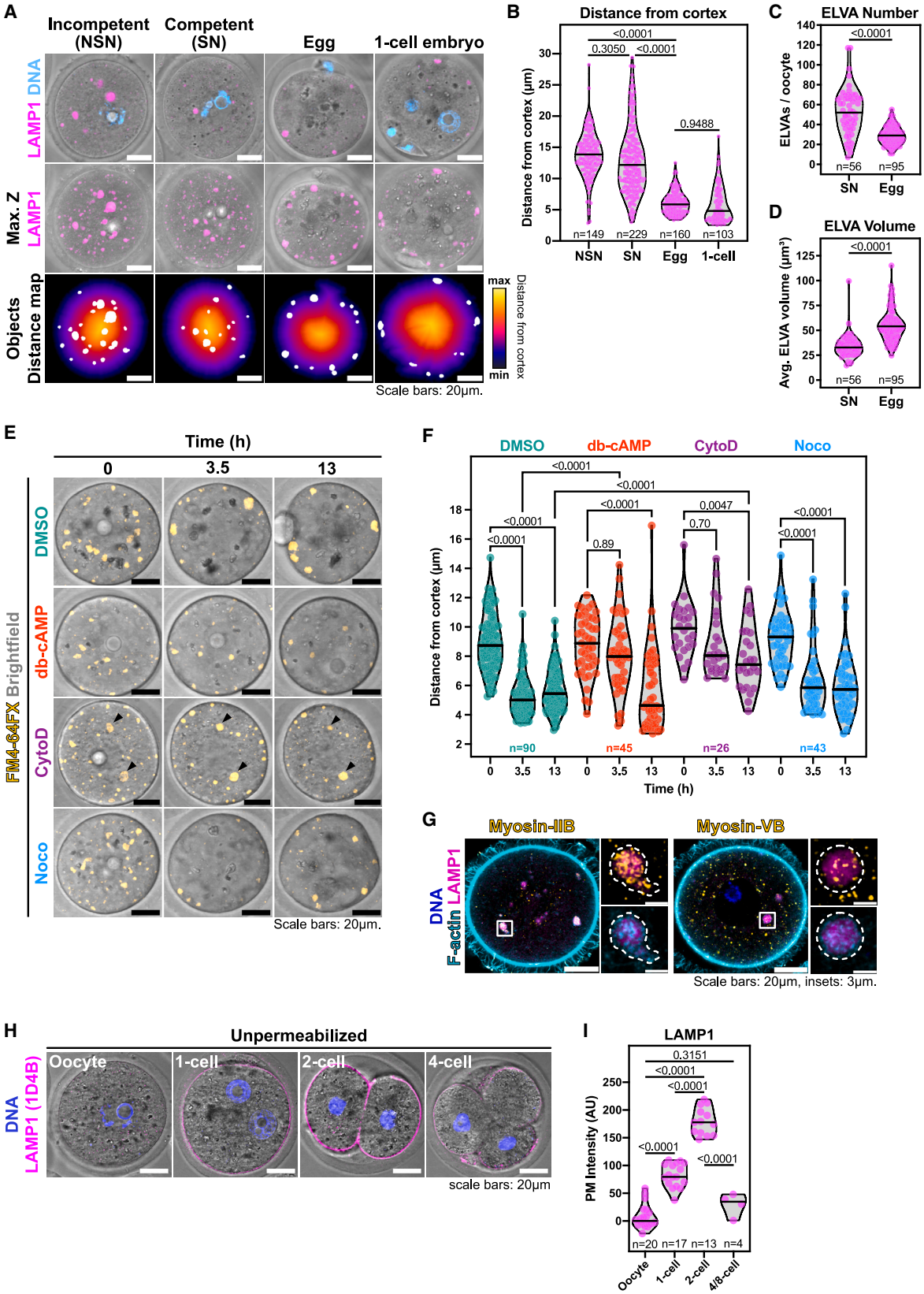

(legend on next page)

FM4-64FX labeling did not significantly affect the oocyte maturation rate nor timing (Figures S2E and S2F). At the time of meiotic resumption and nuclear envelope breakdown (NEBD), ELVAs relocated to the cortex (Figures 2E and 2F; Video S2). To test whether meiosis resumption is required for ELVA relocation, we followed ELVA movements in oocytes treated with db-cAMP, a compound that maintains oocytes arrested in Prophase-I. ELVA corticalization was delayed in db-cAMP-treated oocytes, suggesting that it is indeed coupled to meiotic resumption (Figures 2E and 2F; Video S2).

We next asked whether ELVA relocation depends on the cytoskeleton and followed ELVAs in oocytes treated either with the actin poison cytochalasin D (CytoD) or with the microtubule-depolymerizing drug nocodazole (Noco). Disruption of the actin cytoskeleton with CytoD strongly impaired ELVA movement, whereas in oocytes treated with nocodazole, ELVA behavior was similar to the control (Figures 2E and 2F; Video S2). Thus, we concluded that the cortical movement of ELVAs is actin-dependent. Next, we wanted to gain mechanistic insights into ELVA movement to the cortex. ELVAs contained both actin filaments and myosin motors (Figure 2G). In oocytes, actin nucleators reside on a network of vesicles positive for RAB11, which serve as sites for actin nucleation.[23,24] To test whether ELVAs contain actin-nucleating vesicles and are thus capable of actin nucleation, we injected mRNAs encoding for mCherry-RAB11A into oocytes. mCherry-RAB11A was highly enriched in ELVAs, strongly suggesting that ELVAs contain actin-nucleating vesicles (Figure S2G). In addition, injection of the RAB11A dominant negative mutant S25N, which leads to the loss of RAB11A-positive vesicles in oocytes,[24] completely prevented ELVA relocation (Figure S2H). Together, these data show that ELVAs actively participate in their relocation to the cortex.

Next, we sought to determine the fate of ELVAs during early embryogenesis. It is well known that fertilization results in an increase of cytosolic calcium, which is also a trigger for lysosomal exocytosis.[25,26] Since ELVAs disappear during the first embryonic cleavage (Figures 1A–1C and S1A), we speculated that they may undergo exocytosis following fertilization, benefiting from their cortical localization in eggs (Figures 2A and 2B). To test this, we used a well-established assay for lysosomal exocytosis[27] and immunolabeled unpermeabilized oocytes and embryos with an antibody against the luminal domain of LAMP1 (1D4B; Figures 2H and 2I). Consistent with our hypothesis, LAMP1 appeared on the surface of intact 1-cell embryos and peaked at the 2-cell stage, indicating that lysosomal exocytosis occurs during the first embryonic cleavage (Figures 2H and 2I). We could not detect any LAMP1 on the plasma membrane of immature oocytes, suggesting low or absent lysosomal exocytosis at this stage (Figures 2H and 2I). Interfering with lysosomal exocytosis in zygotes led to the loss of plasma membrane LAMP1 staining (Figures S2I and S2J), accumulation of lysosomes in the embryo (Figures S2K and S2L), and embryonic defects (Figures S2M and S2N). Thus, ELVA dissolution coincides with increased lysosomal exocytosis after fertilization, which is important for proper embryonic development.

Together, these data indicate that ELVAs relocate to the oocyte cortex in an actin-dependent manner following resumption of meiosis and disappear in the 2-cell embryo.

ELVAs are held by a proteinaceous matrix formed by RUFY1

Membranous organelles within ELVAs do not show extensive inter-membrane contacts (Figure 1I; Video S1). Thus, we hypothesized that ELVAs are held together by a proteinaceous matrix and aimed to find the protein glue that holds ELVAs together. Fluorescence-activated particle sorting (FAPS) followed by proteomics has been used to identify the components of non-membrane-bound organelles,[28] but to our knowledge, it has not been tried in vertebrate oocytes before. To probe the feasibility of FAPS in mouse oocytes, we employed the GFP-LC3B transgenic mouse,[29] which has GFP-labeled autophagosomes, to trace ELVAs live (Figures 1K and 3A). We lysed mouse oocytes mechanically and found that ELVAs remained intact upon lysis (Figure 3B). This result motivated us to perform FAPS on oocyte lysates to enrich for ELVAs (Figure 3C). The sorted particles were then analyzed by proteomics to identify the structural organizer of ELVAs. ELVA proteomics revealed several key components of the autophagy-lysosomal pathway, such as LAMP1, RAB7, and cathepsin D as well as ubiquitin, confirming ELVA enrichment in our FAPS experiment (Table S1). A second FAPS experiment performed with non-transgenic wild-type mice also gave similar results (STAR Methods; Figure S3A;

Figure 2. ELVAs relocate to the cortex during oocyte maturation and disappear after fertilization

(A) Top: confocal images of maturation-incompetent (non-surrounded nucleolus, NSN) and -competent (surrounded nucleolus, SN) oocytes, egg, and 1-cell embryo immunolabeled with anti-LAMP1. Middle: maximal Z projections across the equatorial region of each cell. Bottom: masks of the quantified objects overlaid on the distance map.

(B) Quantification of the mean distance of ELVAs from the cell cortex in oocytes, eggs, and embryos. p values: one-way ANOVA with Šidák correction for multiple comparisons.

(C and D) Quantification of ELVA number (C) and average volume (D) in maturation-competent oocytes (SN) and eggs. p values: unpaired t tests with Welch's correction.

(E) Confocal images of mouse oocytes labeled with FM4-64FX and imaged during maturation in presence of the indicated compounds. Black arrowheads in CytoD panel denote the same ELVAs over time. Notice that CytoD-treated oocytes shrink over time. Maximal Z projections across the equatorial region of each oocyte.

(F) Quantification of the average ELVA distance from cortex at the indicated time points in presence of the indicated treatments. p values: one-way ANOVA with Šidák correction for multiple comparisons.

(G) Confocal images of mouse oocytes labeled with anti-LAMP1, phalloidin to highlight F-actin, and the indicated anti-myosin antibodies.

(H) Confocal images of unpermeabilized mouse oocyte and early embryos immunolabeled with an antibody against the luminal domain of LAMP1 (1D4B).

(I) Quantification of the mean plasma membrane intensity of LAMP1 in the experiment shown in (H). Data were normalized subtracting the median of the oocyte sample to all samples. p values: one-way ANOVA with Šidák correction for multiple comparisons.

See also Figure S2.

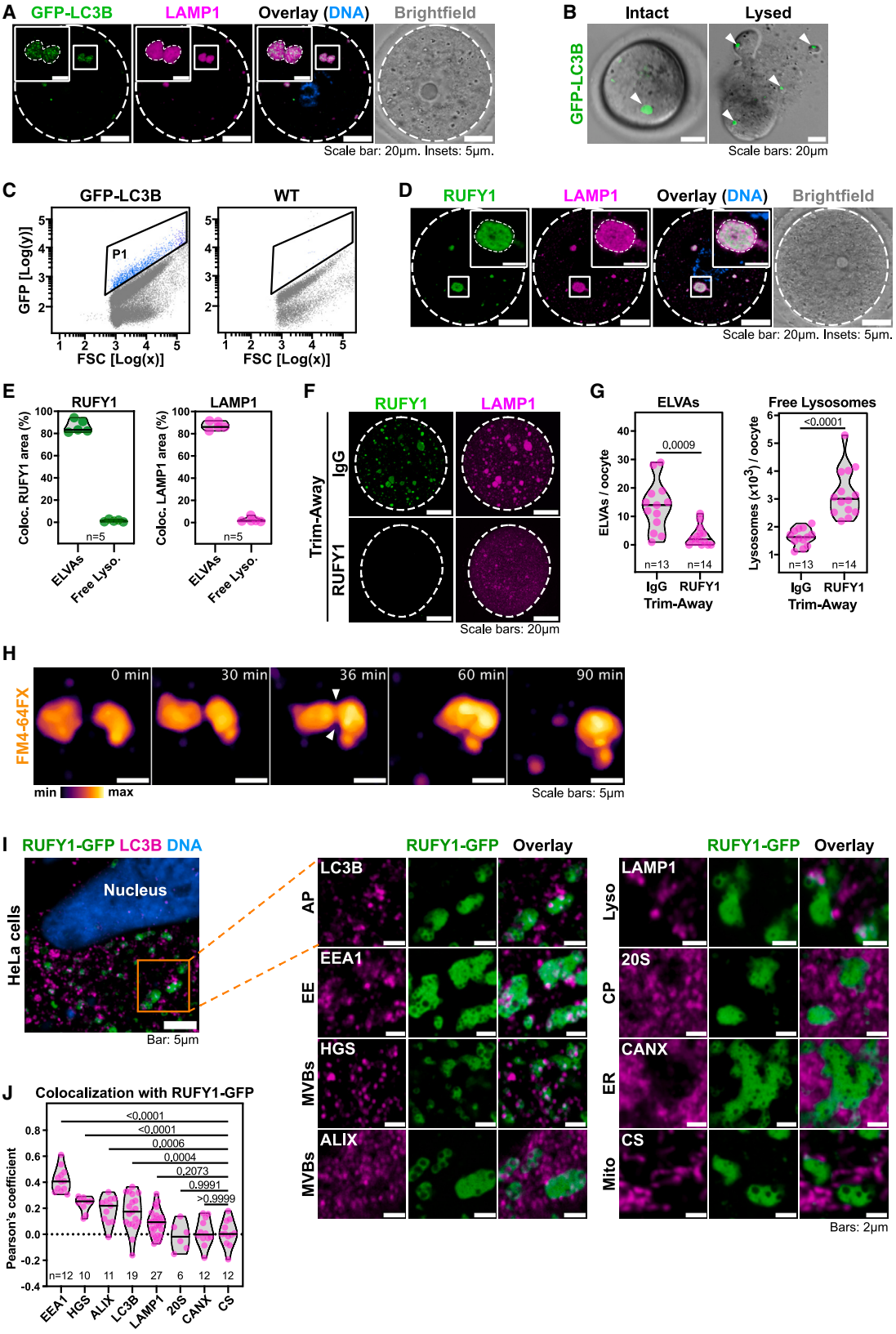

(legend on next page)

Table S1). Subcellular purification of non-membrane-bound compartments, especially when performed using ultra-low input material, inevitably involves cytoplasmic contamination and requires validation. Thus, we moved on to validate the proteins in our list.

Among the ELVA-enriched proteins, we focused on the RUN and FYVE domain-containing protein 1 (RUFY1) as a potential matrix protein because it is highly expressed in oocytes compared with somatic tissues (Figures S3B and S3C), it is a peripheral membrane protein that self-assembles and yields enlarged endosomes upon overexpression,[30–33] and it has an intrinsically disordered domain (IDP) as well as a coiled-coil domain (Figures S3D and S3H), both of which could drive the assembly of non-membrane-bound organelles.[34–38] In addition, family member RUFY4 has been shown to cluster lysosomal vesicles in dendritic cells.[39] To test whether RUFY1 is the structural organizer of ELVAs, we first performed immunofluorescence and found that RUFY1 localizes to ELVAs in oocytes (Figures 3D and 3E). Next, we acutely depleted RUFY1 from oocytes via Trim-Away, an approach to rapidly degrade endogenous proteins in oocytes by injecting a specific antibody against the target protein and an E3-ubiquitin ligase.[40] Trim-Away of RUFY1 resulted in almost complete disappearance of ELVAs (Figures 3F and 3G), indicating that RUFY1 is essential for ELVA integrity. Moreover, the number of LAMP1 puncta in RUFY1-depleted oocytes nearly doubled relative to the control, suggesting that ELVAs sequester a significant portion of the endolysosomal vesicles in oocytes (Figures 3F and 3G). These data indicate that RUFY1 is the matrix protein that holds ELVAs together.

ELVAs do not possess a surrounding membrane, although they contain several membrane-bound organelles (Figures 1I, 1K, and S1G). Non-membrane-bound organelles display a great diversity of physical behaviors, ranging from liquid to solid.[41] To assess material properties of ELVAs, we first looked for fusion events between ELVAs in 4D movies (Figure 3H; Video S3). Separate ELVAs could be seen merging and relaxing into a single object over 1–2 h (Figure 3H; Video S3). Moreover, the number of ELVAs per oocyte decreased during oocyte maturation, whereas the average ELVA volume increased in the same time frame (Figures 1B, 1C, 2C, and 2D). These data suggest that ELVAs undergo extensive fusion with each other during oocyte maturation, albeit over long timescales. To further examine the material properties of ELVAs, we expressed GFP-tagged RUFY1 in oocytes and performed fluorescence recovery after photobleaching (FRAP) experiments. RUFY1-GFP almost exclusively localized to ELVAs (Figures S3E and S3J). FRAP showed that RUFY1-GFP recovered to approximately 60% of the initial fluorescence within 3 min, consistent with the behavior of a dynamic yet viscous liquid (Figures S3F and S3G).

We next wondered whether RUFY1 could act as the driver for ELVA assembly. Overexpression of RUFY1-GFP in somatic cells led to the formation of large, μm-sized compartments, reminiscent of ELVAs in size and shape (Figure 3I). These compartments were also enriched in early and late endosomes,[42] LC3B-positive vesicles (autophagosomes), and to a lesser extent LAMP1-positive vesicles (lysosomes), but they did not contain mitochondria or ER tubules (Figure 3I). 20S proteasome did not appear in these compartments, indicating that some factor may be missing in somatic cells to recruit proteasomes to RUFY1-GFP compartments. Thus, overexpressing RUFY1 is sufficient to drive the formation of ELVA-like compartments in somatic cells that can recruit many of the ELVA-resident vesicles (Figure 3I). To investigate which domain of RUFY1 is critical for matrix formation and self-assembly, we generated RUFY1 deletion mutants in frame with GFP and expressed them in mouse oocytes (Figures S3H and S3I). All deletion constructs still localized to ELVAs, although the coiled coil (ΔCC) and membrane-binding deficient (ΔFYVE) mutants appeared partially diffuse in the cytoplasm compared with the full-length protein (Figures S3I and S3J). ΔCC mutant recovered from photobleaching faster than wild type (Figures S3K and S3L). Moreover, ΔCC mutant was unable to self-assemble in somatic cells and was completely soluble (Figure S3M). These results suggest that the RUFY1 undergoes coiled-coil-mediated self-assembly to drive ELVA formation.

Altogether, these data indicate that ELVAs are viscous non-membrane-bound organelles, the formation of which is driven by RUFY1 self-assembly via its coiled-coil domain.

The degradative activity in ELVAs increases upon oocyte maturation

ELVAs cluster components of both the major intracellular degradative pathways in a super-organelle. We thus asked whether the degradative machinery in ELVAs is regulated.

Figure 3. ELVAs are held together by a RUFY1 matrix

(A) Confocal image of a GFP-LC3B transgenic mouse oocyte immunolabeled with anti-LAMP1. Quantification of the colocalization of GFP-LC3B with ELVAs is shown in Figure 1K.

(B) Representative widefield image of intact and lysed GFP-LC3B transgenic mouse oocytes. Arrowheads indicate ELVAs.

(C) FAPS plots of transgenic GFP-LC3B and wild-type C57BL/6J (WT) oocyte lysates. Particles were sorted for above-background GFP fluorescence (P1).

(D) Confocal image of a mouse oocyte immunolabeled with anti-LAMP1 and anti-RUFY1.

(E) Quantification of the colocalization between RUFY1 and LAMP1 in the experiment shown in (D).

(F) Confocal images of mouse oocytes with or without (IgG) depletion of RUFY1 via TRIM-Away and immunolabeled with anti-LAMP1 and anti-RUFY1. Maximal Z projections across the entire oocyte thickness are shown.

(G) Quantification of ELVAs and lysosome number upon RUFY1 Trim-Away. p values: unpaired t tests with Welch's correction.

(H) Live confocal images of initially separated ELVAs merging into a single object. Arrowheads indicate the initial contact between the two ELVAs.

(I) Representative Airyscan images of HeLa cells transfected with RUFY1-GFP and immunolabeled with the indicated antibodies against organelle markers. EE, early endosomes; MVBs, multivesicular bodies; AP, autophagosomes; lyso, lysosomes; CP, core proteasome (20S); ER, endoplasmic reticulum; Mito, mitochondria.

(J) Quantification of the colocalization between RUFY1-GFP and the organelle markers shown in (I). Numbers indicate the individual cells quantified. p values: one-way ANOVA with Šidák correction for multiple comparisons.

See also Figure S3.

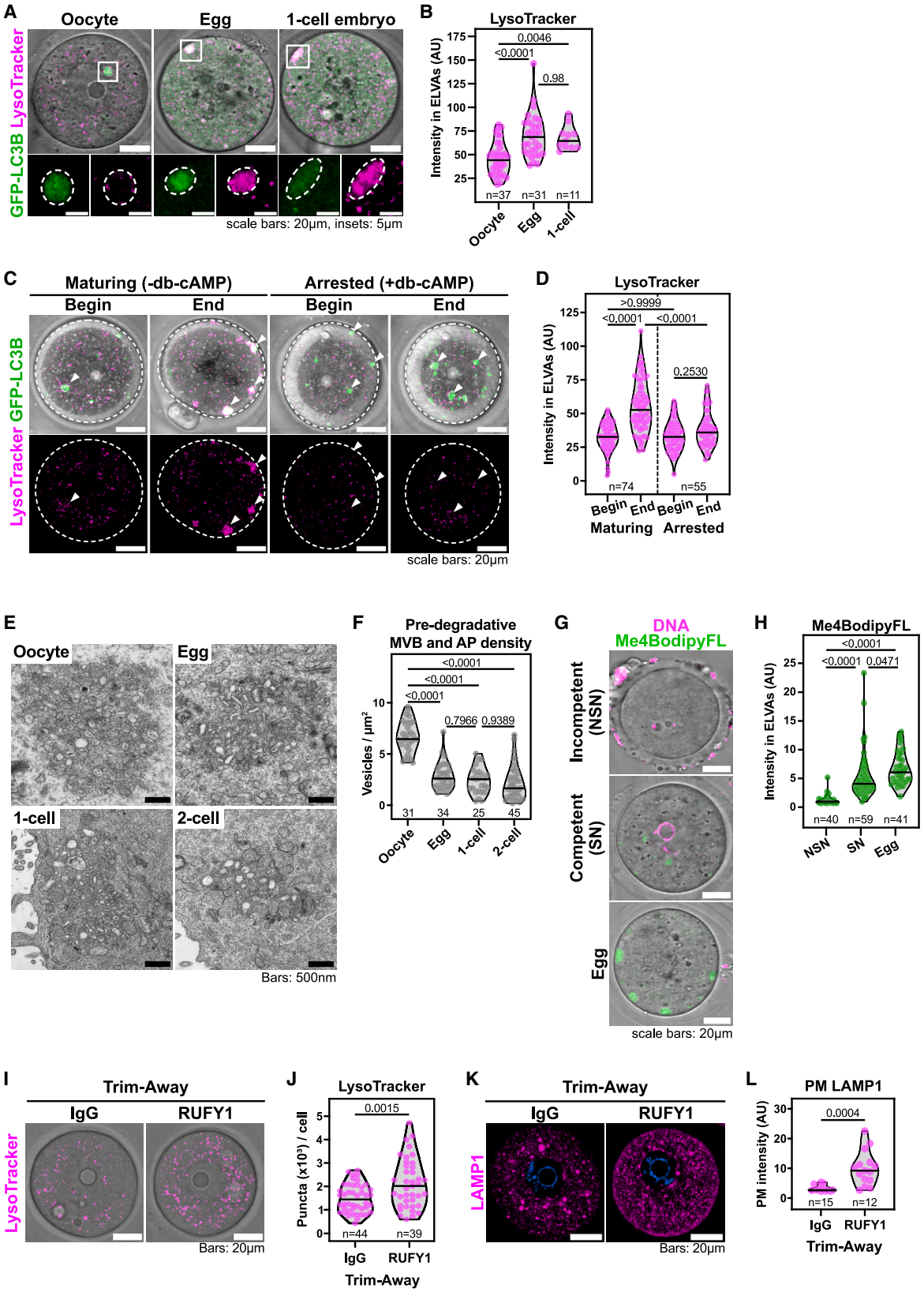

(legend on next page)

We first focused on the autophagy-lysosomal pathway and asked whether lysosomes inside ELVAs are active. We incubated oocytes, eggs, and 1-cell embryos isolated from GFP-LC3B transgenic mice with LysoTracker DeepRed, a probe for acidic, and thus active, lysosomes (Figures 4A and 4B). ELVAs showed little Lysotracker labeling in immature oocytes, suggesting that lysosomes in ELVAs are not active in immature oocytes. Conversely, ELVAs appeared strongly labeled with LysoTracker in eggs and 1-cell embryos, indicating that lysosomes in ELVAs gain degradative activity upon maturation (Figures 4A and 4B). Quantification of the initial and final LysoTracker intensity in individual oocytes imaged live further confirmed that ELVAs accumulated LysoTracker during oocyte maturation (Figures 4C and 4D; Video S4). LysoTracker accumulation was specific since it could be prevented by treatment with Bafilomycin A1 (BafA1), an inhibitor of lysosomal acidification[43,44] (Figures S4A and S4B). Lysotracker intensity did not increase in oocytes whose maturation was inhibited, suggesting that the Lysotracker accumulation in ELVAs during maturation is a specific process (Figures 4C and 4D; Video S4). Further confirmation for these results came from experiments performed with Magic Red, a fluorescent probe that accumulates in active lysosomes upon cleavage by the lysosomal protease Cathepsin B.[45] Magic Red was enriched inside ELVAs in maturing oocytes, indicating that protein degradation is activated in ELVAs during oocyte maturation (Figures S4C and S4D). Thus, we concluded that lysosomes in ELVAs acidify and become degradative during oocyte maturation. Ultrastructural analysis of ELVAs in eggs and 1- and 2-cell embryos also revealed fewer autophagosomes and MVBs after oocyte maturation, while single-membrane vesicles filled with homogeneous material appeared in embryos, suggesting the presence of active lysosomes[18] (Figures 4E and 4F; Video S5). Altogether, these data indicate increased fusion of autophagosomes with lysosomes during oocyte maturation and support that aggregates sequestered within ELVAs are degraded via autophagy during oocyte maturation.

We next asked whether the ubiquitin-proteasome system, the other major protein degradation pathway contained in ELVAs (Figures 1J and 1K), would also be regulated inside ELVAs. To test proteasomal activity, we labeled freshly isolated oocytes and eggs with the proteasomal activity probe Me4BodipyFL. ELVAs increasingly accumulated Me4BodipyFL during the final stages of oocyte growth and maturation (Figures 4G and 4H), suggesting that proteasomal activity increases toward the end of oocyte growth (Figures 4G and 4H). We confirmed the specificity of Me4BodipyFL labeling by treating oocytes with the proteasome inhibitor MG-132 (Figures S4E and S4F). Proteasomal distribution also profoundly changed upon oocyte maturation from a nearly equally cytoplasmic and nuclear distribution in oocytes to mostly nuclear in early embryos (Figures S4G and S4H).

We then asked whether the cortical relocation of ELVAs during oocyte maturation was important for their function. To address this, we blocked ELVA corticalization by disrupting the actin cytoskeleton and examined the activity of the degradative organelles in ELVAs (Figures S4I–S4L). Microtubule-depolymerizing drug Nocodazole was also included as a control to observe the effects of interfering with the cell cycle on the activation of the degradative activity in ELVAs. Both lysosomal acidification and proteasomal activation of ELVAs were significantly reduced when ELVAs could not relocate to the cortex (Figures S4I–S4L). Although we cannot fully exclude that the disruption of actin cytoskeleton could lead to secondary effects, we conclude that movement of ELVAs to the oocyte cortex is important for them to gain degradative activity.

What is the specific function of clustering degradative organelles in ELVAs? To answer this question, we repeated RUFY1 Trim-Away experiments to remove ELVAs in oocytes and investigated the degradative properties of oocytes. Removal of ELVAs triggered lysosomal activation and led to a higher number of active lysosomes in the cytoplasm (Figures 4I and 4J). Moreover, oocytes had premature lysosomal exocytosis concurrent with ELVA disappearance (Figures 4K and 4L). Under unperturbed conditions, ELVA disappearance and lysosomal exocytosis is also coincident but only happens after oocyte maturation (Figures 1A–1C, S1A, 2H, and 2I). Thus, the Trim-Away results reinforced our conclusion that ELVA disappearance is followed by increased lysosomal exocytosis. Altogether, we concluded that ELVAs keep the subset of lysosomes they host in immature

Figure 4. The degradative activity in ELVAs increases during oocyte maturation

(A) Confocal images of a transgenic GFP-LC3B oocyte, egg, and 1-cell embryo labeled with LysoTracker Deep Red.

(B) Quantification of the mean LysoTracker intensity inside ELVAs in the experiment shown in (A). p values: one-way ANOVA with Šidák correction for multiple comparisons.

(C) Confocal images of transgenic GFP-LC3B oocytes imaged during maturation in presence of LysoTracker Deep Red and with or without db-cAMP. Arrowheads indicate ELVAs. Maximal Z projections across the equatorial region of the oocytes.

(D) Quantification of the mean LysoTracker intensity inside ELVAs at the beginning and at the end of oocyte maturation in the experiment shown in (C). p values: one-way ANOVA with Šidák correction for multiple comparisons.

(E) Representative electron micrographs of ELVAs in oocytes, eggs, and 1- and 2-cell embryos.

(F) Quantification of the density of pre-degradative multivesicular bodies (MVB) and autophagosomes (AP) inside ELVAs in the experiment shown in (E). n numbers: individual ELVAs quantified from multiple cells. p values: one-way ANOVA with Šidák correction for multiple comparisons.

(G) Confocal images of maturation-incompetent (NSN), -competent (SN), and mature oocytes (egg) labeled with the proteasome activity probe Me4BodipyFL.

(H) Quantification of the mean Me4BodipyFL intensity inside ELVAs in the experiment shown in (G). Data were normalized to median of maturation-incompetent (NSN) oocytes. p values: one-way ANOVA with Šidák correction for multiple comparisons.

(I) Live confocal images of oocytes with or without depletion of RUFY1 followed by labeling with LysoTracker Deep Red.

(J) Quantification of the intracellular LysoTracker puncta in the experiment shown in (I). p value: unpaired t test with Welch's correction.

(K) Confocal images of oocytes with or without depletion of RUFY1 followed by immunolabeling with anti-LAMP1.

(L) Quantification of the plasma membrane (PM) intensity of LAMP1 in the experiment shown in (K). p value: unpaired t test with Welch's correction.

See also Figure S4.

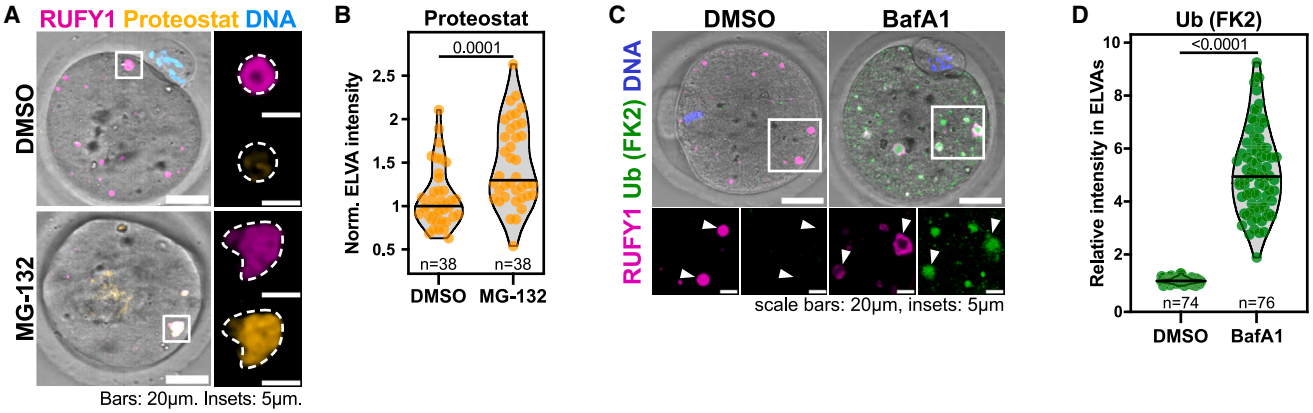

Figure 5. ELVAs degrade aggregated proteins upon oocyte maturation

(A) Confocal images of mouse oocytes treated with or without the proteasome inhibitor MG-132 during maturation and labeled with Proteostat and anti-LAMP1.

(B) Quantification of the mean Proteostat intensity inside ELVAs in the experiment shown in (A). Data were normalized to the median of the DMSO sample. p value: unpaired t test with Welch's correction.

(C) Confocal images of mouse oocytes *in vitro* matured with or without the lysosomal inhibitor bafilomycin A1 (BafA1) and immunolabeled with anti-RUFY1 and anti-ubiquitin conjugates (FK2).

(D) Quantification of the mean ubiquitin intensity inside ELVAs in the experiment shown in (C). Data were normalized to the median of the DMSO sample. p value: unpaired t test with Welch's correction.

oocytes inactive, and their forced removal prematurely activates lysosomes and leads to premature lysosomal exocytosis.

The fact that protein aggregates are present in immature oocytes but disappear in early embryos (Figures 1A and 1H) coincident with activation of the degradative activity in ELVAs (Figures 4A–4H) suggests that aggregates sequestered within ELVAs are degraded upon oocyte maturation. Confirming this hypothesis, aggregated proteins strongly accumulated in ELVAs in the presence of the proteasome inhibitor MG-132 (Figures 5A and 5B). Similarly, treatment of maturing oocytes with the lysosomal inhibitor BafA1 significantly increased the levels of ubiquitinated proteins in ELVAs (Figures 5C and 5D).

Taken together, our data show that ELVAs are not degradative in maturation-incompetent oocytes, but they have degradative activity in mature eggs after activation of both the major protein degradation routes, the ubiquitin-proteasome system and autophagy.

ELVAs clear detrimental protein aggregates upon oocyte maturation

Our data so far suggest that ELVAs function to sequester proteins and degrade them only upon oocyte maturation. To directly test this idea, we sought to identify specific proteins that are sequestered in ELVAs in immature oocytes and ask whether they are subsequently degraded as oocytes mature. To identify such proteins, we performed proteomics on lysosome-inhibited (BafA1-treated) and untreated oocytes (Table S2) and combined this list with the list of ELVA-enriched proteins to find out possible ELVA cargos (Table S3). Among possible top candidates (Table S3), we concentrated on two proteins whose aberrant expression is frequently associated with pathologies: the mast/stem cell growth factor receptor KIT, a proto-oncogene whose expression is tightly controlled during oocyte growth and early embryogenesis,[46,47] and the TAR DNA-binding protein 43 (TDP-43), an RNA-binding protein well known for aggregating in neurodegenerative diseases[48] and found to be highly ubiquitinated in eggs.[49]

Using immunofluorescence, we could indeed show that both KIT and TDP-43 were found in ELVAs in immature oocytes when ELVAs do not have degradative activity (Figures 6A–6D). KIT and TDP-43 levels in ELVAs declined upon oocyte maturation and became undetectable in 1- and 2-cell embryos (Figures 6A–6D). We confirmed that TDP-43 and KIT are degraded inside ELVAs by showing that inhibition of lysosomal degradation during oocyte maturation prevented the decline of TDP-43 and KIT levels (Figures 6E–6H). Importantly, although soluble TDP-43 is degraded mainly by the ubiquitin-proteasome system, aggregated TDP-43 is targeted by the autophagy-lysosomal pathway.[50] The fact that TDP-43 levels increased inside ELVAs upon lysosomal inhibition (Figures 6G and 6H) indicates that its accumulation in ELVAs is due to aggregation. To ensure that ELVAs are a degradation route for specific (i.e., aggregated) proteins, rather than a common protein degradation route, we looked at localization patterns for proteins that are highly expressed in oocytes and degraded upon oocyte maturation.[51–53] We recapitulated the existing literature showing that the protein levels of ZAR1, LSM14B, and G3BP2 decrease significantly upon oocyte maturation[51–53] (Figures S5A–S5F). However, all three proteins were excluded from ELVAs (Figures S5D–S5F). Therefore, we concluded that ELVAs represent a specific, rather than generic, protein degradation route.

Taking all this together, we concluded that ELVAs degrade specific sequestered proteins, including disease-linked TDP-43 and KIT, upon oocyte maturation.

The fact that aggregated proteins in ELVAs are degraded at maturation suggests that the presence of protein aggregates could interfere with egg and embryo quality and that oocytes need to clear them before developing into an egg. We tested

CellPress
OPEN ACCESS

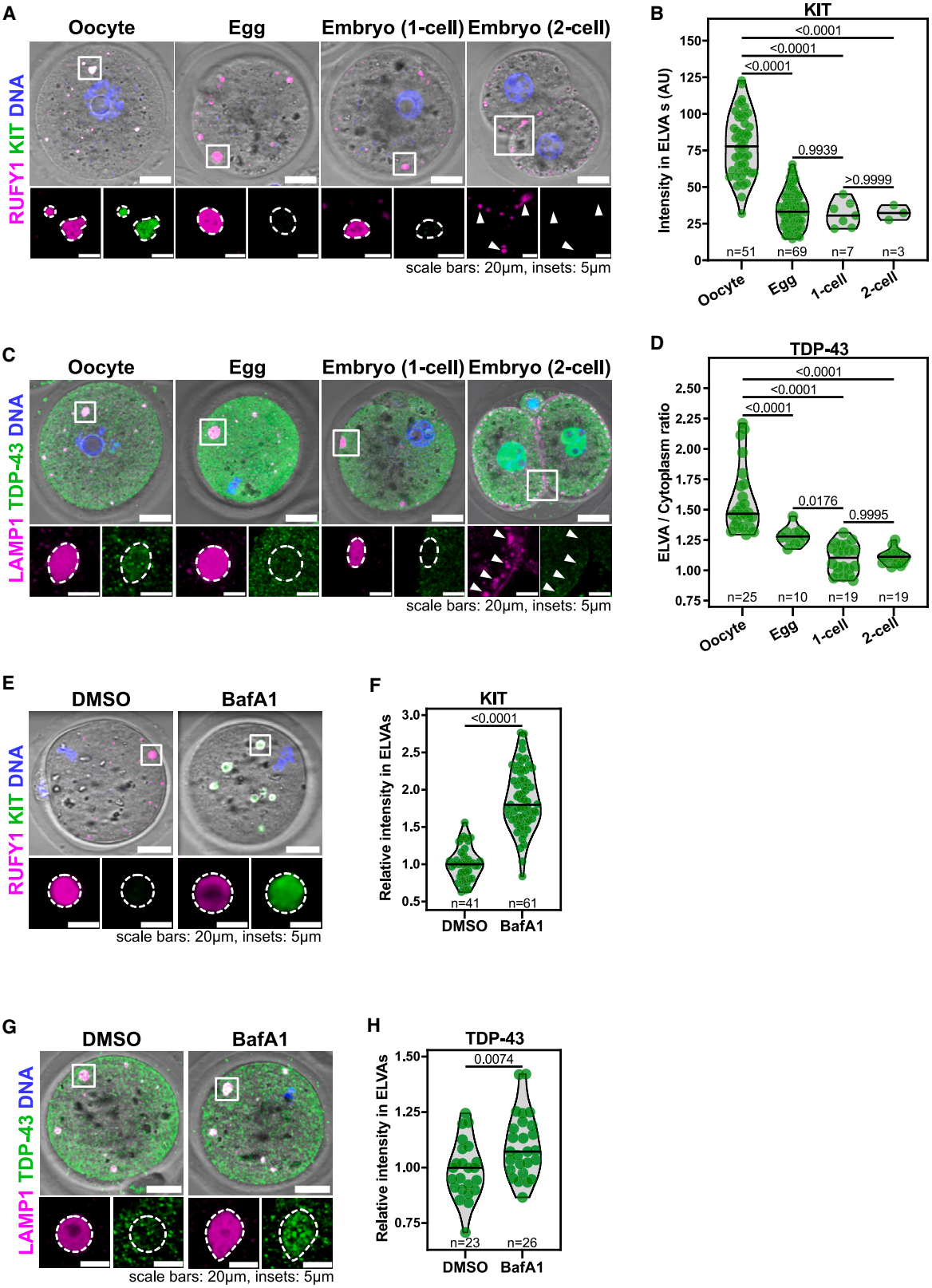

(legend on next page)

this idea by showing that preventing lysosomal degradation during oocyte maturation causes accumulation of aggregates in ELVAs (Figures 5A–5D) and leads to the formation of defective eggs (Figures 7A, 7B, and S6A). Although this treatment will affect all lysosomes, since 40% to 80% of lysosomes are in ELVAs (Figures 3G, S6B, and S6C), we reasoned that any effects would be mainly associated with the function of ELVAs. Non-invasive imaging of proteasomal activity also showed that oocytes with low proteasomal activity in ELVAs did not mature or had severe maturation problems (Figures 7C–7F). Thus, we conclude that clearing the aggregated proteins in ELVAs during oocyte maturation is essential to produce high-quality eggs.

We then asked what happens if the embryos fail to clear aggregated proteins. We treated 1-cell embryos with BafA1 to inhibit protein degradation, then washed the inhibitor after the first embryonic cleavage and allowed the embryos to develop until the blastocyst stage. As expected, ubiquitinated proteins remained inside ELVAs in 2-cell embryos after BafA1 treatment (Figures 7G and 7H). Remarkably, the majority (~60%) of the treated embryos that retained aggregates in ELVAs failed to develop to blastocyst stage (Figures 7I and 7J), suggesting that the clearance of protein aggregates is essential for healthy embryonic development.

Next, to directly test whether protein aggregates are detrimental for the embryo, we injected zygotes with mRNAs encoding for aggregating proteins: first, we used a well-characterized aggregating TDP-43 mutant without an NLS to minimize interfering with zygotic genome activation (M337V ΔNLS).[48,54,55] To exclude any effects that could be due to the overexpression of TDP-43 rather than its aggregation, we repeated injections with a synthetic protein designed to aggregate (AgDD-GFP).[56] Both constructs led to the formation of aggregates inside embryos (Figures 7K and S6D). We confirmed that these aggregates were ubiquitinated (Figures 7L and S6E). The presence of protein aggregates severely disrupted early embryonic development beyond the 2-cell stage and caused rapid embryonic death (Figures 7M, 7N, and S6F). Thus, we concluded that protein aggregates are detrimental for embryonic survival.

Together, our data show that mouse oocytes contain a previously uncharacterized (super)organelle that hosts components of the two major intracellular degradative pathways. Immature oocytes have lower overall proteasomal activity and more inactive lysosomes in ELVAs compared with mature oocytes and embryos. In immature oocytes, ubiquitinated and aggregated proteins are sequestered within ELVAs until the final stages of oocyte growth and maturation. ELVAs therefore represent a proteostatic strategy in which protein aggregates are sequestered until degradative activity increases during oocyte maturation, allowing eggs to clear protein aggregates and develop into viable embryos.

DISCUSSION

The question of how cells deal with protein aggregates is central to understanding their long-term health. Long-lived cells have a particular problem, as they cannot use cell division to clear protein aggregates,[57] whose build-up is correlated with numerous diseases. Here, we have shown that mammalian oocytes also accumulate protein aggregates during their long life. Our data show that unexpectedly, immature oocytes have lower proteasomal and lysosomal activity and sequester aggregated proteins in specialized super-organelles but only degrade them at final stages of oocyte growth and maturation. Previous studies elegantly demonstrated that autophagy is essential for early embryogenesis, but not for oocyte growth.[4,5] Our findings corroborate these results and suggest that the reason for the 2-cell stage arrest in autophagy-deficient embryos could be a failure to clear protein aggregates, as embryos with protein aggregates fail to develop beyond 2-cell stage. Our data also offer an explanation for how growing oocytes can seemingly dispense with autophagy: clearing protein aggregates from the oocyte cytoplasm is achieved after oocyte maturation, and thus, autophagy only becomes essential after maturation.

Why would oocytes keep aggregated proteins sequestered to degrade them at maturation? Immature oocytes lack major metabolic routes that would likely impact efficient ATP generation.[58] Lysosomes, proteasomes, and other components of the degradative machinery require large amounts of energy to remain active.[59,60] Therefore, we speculate that this "store to degrade later" strategy to deal with aggregated proteins ensures that toxic aggregates are kept separate from the oocyte cytoplasm while lowering the energy spent to keep an aggregate-free cytoplasm during the long life of the oocyte. Moreover, storing aggregated proteins in ELVAs would preserve raw materials for the rapid embryonic divisions, when they will be needed the

Figure 6. ELVA cargos include disease-linked and aggregated proteins essential for oocyte and embryo development

(A) Confocal images of a mouse oocyte, egg, and 1- and 2-cell embryos immunolabeled with anti-RUFY1 and anti-KIT.

(B) Quantification of the mean KIT intensity inside ELVAs in the experiment shown in (A). p values: one-way ANOVA with Šidák correction for multiple comparisons.

(C) Confocal images of a mouse oocyte, egg, 1- and 2-cell embryos immunolabeled with anti-LAMP1 and anti-TDP-43.

(D) Quantification of the mean TDP-43 enrichment in ELVAs in the experiment shown in (C). p values: one-way ANOVA with Šidák correction for multiple comparisons.

(E) Confocal images of mouse oocytes treated with or without BafA1 during maturation and immunolabeled with anti-RUFY1 and anti-KIT.

(F) Quantification of the mean KIT intensity inside ELVAs in the experiment shown in (E). Data were normalized to the median of DMSO. p values: unpaired t test with Welch's correction.

(G) Confocal images of mouse oocytes treated with or without BafA1 during maturation and immunolabeled with anti-LAMP1 and anti-TDP-43.

(H) Quantification of the mean TDP-43 intensity inside ELVAs in the experiment shown in (G). Data were normalized to the median of DMSO. p values: unpaired t test with Welch's correction.

See also Figure S5.

CellPress
OPEN ACCESS

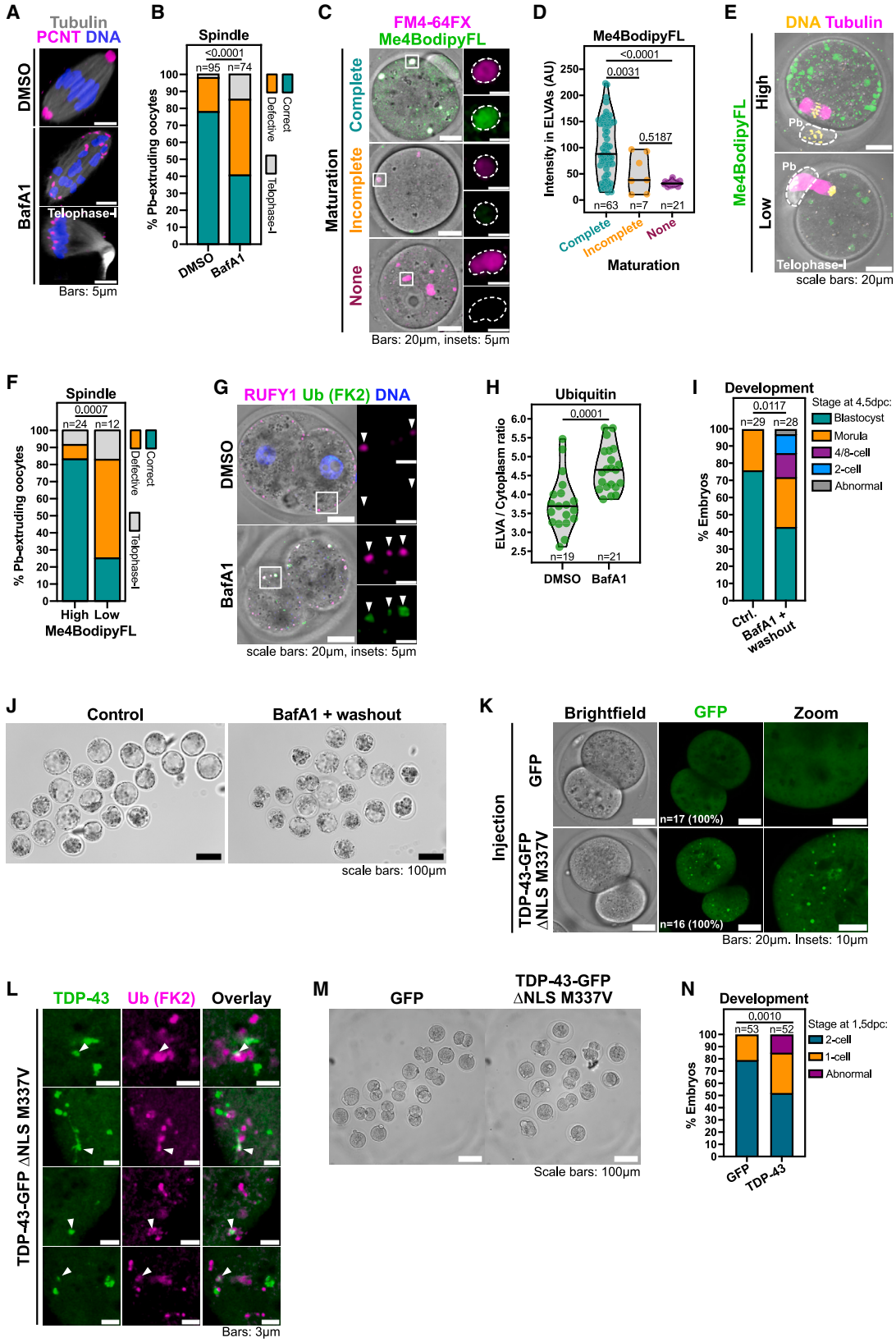

(legend on next page)

most. This way, the oocyte could ensure that the new embryo is replenished with building blocks such as amino acids and would be more resilient in its immediate growth conditions.

Several studies came across ELVAs in their examinations of oocytes and eggs but interpreted them to be endosomes,[61] amphisomes,[62] "aggregated vesicles from the endomembrane system,"[49] or ATG9-positive vesicles.[63] Although all these papers correctly identified components of ELVAs, they missed recognizing ELVAs as standalone compartments clustering all these vesicles and more components (Figures 1I–1K, S1G, S1I, and S1J). Indeed, ELVAs represent a spatial organization of endolysosomal trafficking that involves tightly packed vesicles in a condensed liquid-like compartment. Our data indicate that the clustering of degradative organelles embedded in a RUFY1 matrix inside ELVAs can suppress their activity: lysosomes within ELVAs are not acidic in immature oocytes and thus not degradative, but they become acidic upon ELVA removal by RUFY1 TrimAway. How the oocyte maintains a different pool of cytoplasmic and ELVA-resident organelles is an intriguing direction for future studies. For instance, lysosome acidification is mostly achieved via vacuolar (V)-type ATPases, which use ATP to generate a pH gradient.[59] Recent studies on lysosomal heterogeneity suggest that V-ATPase assembly at lysosomes is a mechanism for achieving differential lysosomal activity within the same cell.[64] It is possible that ELVA-resident lysosomes do not have V-ATPases by passive (i.e., sequestration in a protein matrix) or active (i.e., RUFY1- or mTORC1-dependent)[42,65] mechanisms that are overridden after oocyte maturation. We also find proteasomes have low activity in growing oocytes. This downregulation of proteasomal activity is not due to core subunit levels, as oocytes and eggs have similar levels of the core 20S subunits (Figures S4G and S4H; Li et al.[52]). Thus, we speculate that mechanisms such as the presence of small inhibitory peptides and/or 19S subunit assembly play a role in the regulation of proteasomal activity in early embryogenesis.

The other similar paradigm of tightly packed vesicles in a liquid-like compartment was suggested for synapses, where synaptic vesicles are organized in a liquid phase.[66] We speculate that the liquid phases of ELVAs and synapses are necessary for the trafficking of vesicles in and out of these compartments without a need for an anchorage site. This way, ELVAs can sequester aggregated proteins freely in the cytoplasm during the long life of the oocyte.

ELVAs add to the intriguing mechanisms oocytes employ to keep their cytoplasm healthy: unlike those of vertebrates, the early oocytes of *Caenorhabditis elegans* (*C. elegans*) do not have active lysosomes and increasingly accumulate protein aggregates in their cytoplasm as they grow.[67,68] However, when maturing oocytes get closer to the sperm of the hermaphrodite animal, the lysosomes in *C. elegans* oocytes get activated upon sperm signaling and clear the cytoplasmic aggregates.[67] Despite the different evolutionary constraints between *C. elegans* and mouse oocytes (i.e., worms have constant oocyte generation with short-lived oocytes, whereas most mammalian oocytes are formed before birth and are long-lived), it is fascinating that both animals have evolved similar strategies to ensure the passage of damage-free cytoplasm to their offspring.

Poor oocyte quality is a major cause of female infertility. The most studied oocyte defects are spindle assembly and positioning problems, as they frequently lead to aneuploidy and, in turn, to unviable embryos.[1] However, a recent review of euploid embryo transfers found out that other unknown factors are also vital for embryo survival.[69] Indeed, the number of "large LC3 puncta"—which are likely ELVAs—increases with age in mouse oocytes.[62] Our research opens a fascinating future direction to

Figure 7. Protein aggregates are detrimental for egg quality and embryo survival

(A) Confocal images (3D projections) of mouse metaphase-II (MII) spindles from oocytes *in vitro* matured with or without BafA1 and immunolabeled with anti-tubulin and anti-pericentrin (PCNT).

(B) Quantification of spindle characteristics in the experiment shown in (A). Spindles were considered correct when chromosomes were aligned on a central plate and PCNT signal was at the spindle poles. p value: Fischer's exact test.

(C) Live confocal images of *in vitro* matured mouse oocytes labeled with FM-4-64FX and with the proteasome activity probe Me4BodipyFL. Maturation was considered complete if a polar body (PB) was extruded, incomplete if nuclear envelope breakdown (NEBD) occurred but no PB was extruded, and none if NEBD did not occur.

(D) Quantification of the mean Me4BodipyFL intensity inside ELVAs in the experiment shown in (C). p values: one-way ANOVA with Šidák correction for multiple comparisons.

(E) Live confocal images of *in vitro* matured mouse oocytes labeled with Me4BodipyFL, SPY555-Tubulin, and SiR-DNA. Pb, polar body.

(F) Quantification of the spindle morphology and positioning in the experiment shown in (E). Spindles adjacent and parallel to the cortex with chromosomes aligned on a central plate were considered correct; otherwise, they were considered defective. p value: Fischer's exact test.

(G) Confocal images of mouse embryos treated with or without BafA1 during the first embryonic cleavage and immunolabeled with anti-RUFY1 and anti-ubiquitin conjugates (FK2).

(H) Quantification of the mean ubiquitin enrichment inside ELVAs in the experiment shown in (G). p values: unpaired t test with Welch's correction.

(I) Quantification of the embryonic development rate of mouse 1-cell embryos treated with or without BafA1 during the first embryonic cleavage, followed by BafA1 washout, and cultured until blastocyst stage. Development was assessed at 4.5 dpc (days post coitum). Blastocysts were counted based on the presence of a blastocoel, irrespective of embryo morphology. p value: Fischer's exact test.

(J) Representative widefield images of mouse embryos treated as described in (I). Images were taken at 4.5 dpc.

(K) Live confocal images of embryos injected with GFP or TDP-43-GFP ΔNLS M337V mRNA and imaged after the first embryonic cleavage.

(L) Representative confocal images of embryos injected with TDP-43-GFP ΔNLS M337V mRNA and immunolabeled with anti-Ub FK2. Arrowheads indicate ubiquitinated aggregates.

(M) Representative widefield image of embryos injected with GFP or TDP-43-GFP ΔNLS M337V mRNA and imaged after the first embryonic cleavage.

(N) Quantification of development after one overnight culture in embryos injected with GFP or TDP-43-GFP ΔNLS M337V mRNA. p value: Fischer's exact test. See also Figure S6.

explore whether protein degradation and its (mis)regulation in oocytes could help explain the age-related decline in embryo health.

Could ELVA-like compartments exist in other cell types? Quiescent stem cells are long-lived cells that do not divide often. Recently, hematopoietic stem cells (HSCs) were found to traffic their misfolded proteins into special compartments called aggresomes to store them until HSCs are activated to divide.[70] Thus, aggresomes in HSCs have a striking functional similarity to ELVAs in oocytes, although they differ in their composition. Neurons also have aggregated proteins in the vicinity of proteasomes or membranous organelle clusters.[71] How these long-lived cells preferentially traffic their aggregated proteins into specialized compartments and regulate their degradation, and whether this compartmentalization also plays an important role in neurons, remain future research avenues to explore.

Limitations of the study

We acknowledge that inhibiting lysosomal degradation in the whole oocyte could affect several pathways, but we reason that it would mostly reflect ELVAs' function, as they contain a large fraction of the total lysosomes in the oocyte (Figures 3G, S6B, and S6C).

We refrained from inhibiting proteasomal activity during oocyte maturation, as it is essential for meiotic progression.[72] Instead, we checked whether there is a correlation between the activity of proteasomes in ELVAs and egg quality and labeled *in vitro* matured oocytes with the proteasomal activity probe Me4BodipyFL (Figures 7C–7F). Oocytes that completed maturation strongly accumulated Me4BodipyFL in ELVAs, whereas those that did not mature showed little to no Me4BodipyFL accumulation (Figures 7C and 7D). We next speculated that low proteasomal activity in ELVAs could lead to maturation problems and, thus, to defective eggs. Indeed, >70% of oocytes with low Me4BodipyFL labeling in ELVAs displayed spindle defects (Figures 7E and 7F). Thus, we concluded that high proteasomal activity in ELVAs during oocyte maturation correlates with better egg quality.

Finally, our data do not rule out the possibility that oocytes may employ mechanisms to reduce protein aggregation during their long lives.

STAR★METHODS

Detailed methods are provided in the online version of this paper and include the following:

- KEY RESOURCES TABLE
- RESOURCE AVAILABILITY
  - Lead contact
  - Materials availability
  - Data and code availability
- EXPERIMENTAL MODEL AND STUDY PARTICIPANT DETAILS
  - Mice
  - Cell lines
  - Bacterial Strains
- METHOD DETAILS
  - Oocytes, eggs and embryo collection and culture
  - Drugs, dyes and other live treatments
  - Mouse oocyte cDNA library preparation
  - DNA Constructs
  - *In vitro* transcription and mRNA injection
  - Trim-Away
  - Live imaging of oocytes
  - FRAP
  - Transfection and imaging of cultured cells
  - Immunofluorescence of oocytes and embryos
  - Immunofluorescence of cultured cells
  - Immunohistochemistry
  - Electron microscopy
  - Mass Spectrometry
  - Western Blotting
- QUANTIFICATION AND STATISTICAL ANALYSIS

SUPPLEMENTAL INFORMATION

Supplemental information can be found online at https://doi.org/10.1016/j.cell.2024.01.031.

ACKNOWLEDGMENTS

We would like to thank Michaela Wilsch-Bräuninger and Weihua Leng (MPI-CBD EM facility, Dresden) for processing the samples for EM and acquiring the images and for critical comments on the manuscript. We are grateful to the CRG/UPF Proteomics and the CRG Advanced Light Microscopy Unit for the support and assistance in this work. We are also grateful to the PRBB Animal Facility for assistance with animal care. TDP-43 plasmids were a kind gift from the Hyman lab. We further acknowledge Marina Carmona Rivas for assistance with cloning RUFY1-GFP constructs and the CRG Tissue Engineering Unit and Marta Miret Cuesta (Irimia lab, CRG) for assistance with oocyte and embryo injections. Finally, we are grateful to Sascha Martens, Vivek Malhotra, Nicholas Stroustrup, Ishier Raote, and Ben Lehner for their comments on the manuscript. We acknowledge the support of the Spanish Ministry of Science and Innovation through the Centro de Excelencia Severo Ochoa (CEX2020-001049-S, MCIN/AEI/10.13039/501100011033) and the Generalitat de Catalunya through the CERCA program. G.Z. received funding from the European Union's Horizon 2020 research and innovation program under the Marie Skłodowska-Curie grant agreement no. 754422. E.B. acknowledges funding from the Ministerio de Ciencia e Innovación PID2020-115127GB-I00, the European Research Council Starting Grant (ERC-StG-2017-759107), and the Vallee Scholar Award (Vallee Foundation Inc.). The work of S.C. and M.S. was supported by the Max Planck Society and the Deutsche Forschungsgemeinschaft (DFG, German Research Foundation) under Germany's Excellence Strategy (EXC 2067/1-390729940) and a DFG Leibniz Prize to M.S. (SCHU 3047/1-1). S.C. was additionally supported by a European Molecular Biology Organization long-term postdoctoral fellowship.

AUTHOR CONTRIBUTIONS

G.Z. and S.C. independently performed the initial characterization of ELVAs in the laboratories of E.B. and M.S., respectively. G.Z. designed the study, performed most of the experiments, analyzed the data, and prepared the figures. S.C. performed RUFY1 TRIM-Away experiments, Proteostat labeling in CD1 and FvB/N oocytes, RAB11 injections, and ZAR1 immunofluorescence under the supervision of M.S. M.C.S. performed the FAPS. B.P. performed RUFY1-GFP mutants' injection in oocytes under the supervision of M.I. J.M.D. performed the experiments with cultured cells. E.B. supervised the project. G.Z. and E.B. wrote the manuscript with input from all co-authors.

DECLARATION OF INTERESTS

The authors declare no competing interests.

Received: June 7, 2023
Revised: December 4, 2023
Accepted: January 19, 2024
Published: February 20, 2024

REFERENCES

1. Charalambous, C., Webster, A., and Schuh, M. (2023). Aneuploidy in mammalian oocytes and the impact of maternal ageing. Nat. Rev. Mol. Cell Biol. *24*, 27–44.
2. Dikic, I. (2017). Proteasomal and Autophagic Degradation Systems. Annu. Rev. Biochem. *86*, 193–224.
3. Lowe, J., Blanchard, A., Morrell, K., Lennox, G., Reynolds, L., Billett, M., Landon, M., and Mayer, R.J. (1988). Ubiquitin is a common factor in intermediate filament inclusion bodies of diverse type in man, including those of Parkinson's disease, Pick's disease, and Alzheimer's disease, as well as Rosenthal fibres in cerebellar astrocytomas, cytoplasmic bodies in muscle, and mallory bodies in alcoholic liver disease. J. Pathol. *155*, 9–15.
4. Tsukamoto, S., Kuma, A., Murakami, M., Kishi, C., Yamamoto, A., and Mizushima, N. (2008). Autophagy Is Essential for Preimplantation Development of Mouse Embryos. Science *321*, 117–120.
5. Song, Z.H., Yu, H.Y., Wang, P., Mao, G.K., Liu, W.X., Li, M.N., Wang, H.N., Shang, Y.L., Liu, C., Xu, Z.L., et al. (2015). Germ cell-specific Atg7 knockout results in primary ovarian insufficiency in female mice. Cell Death Dis. *6*, e1589.
6. Shen, X.H., Jin, Y.X., Liang, S., Kwon, J.W., Zhu, J.W., Lei, L., and Kim, N.H. (2018). Autophagy is required for proper meiosis of porcine oocytes maturing in vitro. Sci. Rep. *8*, 12581.
7. Sánchez, M.L.E., Martínez, O.M.E., and Vázquez-Nin, G.H. (2012). Immunohistochemical and ultrastructural visualization of different routes of oocyte elimination in adult rats. Eur. J. Histochem. *56*, e17.
8. Herbert, M., Levasseur, M., Homer, H., Yallop, K., Murdoch, A., and McDougall, A. (2003). Homologue disjunction in mouse oocytes requires proteolysis of securin and cyclin B1. Nat. Cell Biol. *5*, 1023–1025.
9. Hipp, M.S., Kasturi, P., and Hartl, F.U. (2019). The proteostasis network and its decline in ageing. Nat. Rev. Mol. Cell Biol. *20*, 421–435.
10. Wilson, D.M., Cookson, M.R., Van Den Bosch, L.V.D., Zetterberg, H., Holtzman, D.M., and Dewachter, I. (2023). Hallmarks of neurodegenerative diseases. Cell *186*, 693–714.
11. Sala, A.J., and Morimoto, R.I. (2022). Protecting the future: balancing proteostasis for reproduction. Trends Cell Biol. *32*, 202–215.
12. Leeman, D.S., Hebestreit, K., Ruetz, T., Webb, A.E., McKay, A., Pollina, E.A., Dulken, B.W., Zhao, X., Yeo, R.W., Ho, T.T., et al. (2018). Lysosome activation clears aggregates and enhances quiescent neural stem cell activation during aging. Science *359*, 1277–1283.
13. Lee, Y., Kim, J., Kim, M.S., Kwon, Y., Shin, S., Yi, H., Kim, H., Chang, M.J., Chang, C.B., Kang, S.B., et al. (2021). Coordinate regulation of the senescent state by selective autophagy. Dev. Cell *56*, 1512–1525.e7.
14. Ray, S., Singh, N., Kumar, R., Patel, K., Pandey, S., Datta, D., Mahato, J., Panigrahi, R., Navalkar, A., Mehra, S., et al. (2020). α-Synuclein aggregation nucleates through liquid–liquid phase separation. Nat. Chem. *12*, 705–716.
15. Ho, Y., Wigglesworth, K., Eppig, J.J., and Schultz, R.M. (1995). Preimplantation development of mouse embryos in KSOM: Augmentation by amino acids and analysis of gene expression. Mol. Reprod. Dev. *41*, 232–238.
16. Preis, K.A., Seidel, G., and Gardner, D.K. (2005). Metabolic markers of developmental competence for in vitro-matured mouse oocytes. Reproduction *130*, 475–483.
17. Miao, Y., Ma, S., Liu, X., Miao, D., Chang, Z., Luo, M., and Tan, J. (2004). Fate of the first polar bodies in mouse oocytes. Mol. Reprod. Dev. *69*, 66–76.
18. Klumperman, J., and Raposo, G. (2014). The Complex Ultrastructure of the Endolysosomal System. Cold Spring Harb. Perspect. Biol. *6*, a016857.
19. Yamada, E., Muta, T., Muta, T., Koga, H., Motomura, A., D., M., Koga, H., and D., M. (1957). The fine structure of the oocyte in the mouse ovary studied with electron microscope. Kurume Med. J. *4*, 148–171.
20. Wischnitzer, S. (1970). An electron microscope study of cytoplasmic organelle transformations in developing mouse oocytes. Wilhelm Roux. Arch. Entwickl. Mech. Org. *166*, 150–172.
21. Merchant, H., and Chang, M.C. (1971). An electron microscopic study of mouse eggs matured *in vivo* and *in vitro*. Anat. Rec. *171*, 21–37.
22. Wassarman, P.M., and Josefowicz, W.J. (1978). Oocyte development in the mouse: An ultrastructural comparison of oocytes isolated at various stages of growth and meiotic competence. J. Morphol. *156*, 209–235.
23. Schuh, M. (2011). An actin-dependent mechanism for long-range vesicle transport. Nat. Cell Biol. *13*, 1431–1436.
24. Holubcová, Z., Howard, G., and Schuh, M. (2013). Vesicles modulate an actin network for asymmetric spindle positioning. Nat. Cell Biol. *15*, 937–947.
25. Clift, D., and Schuh, M. (2013). Restarting life: fertilization and the transition from meiosis to mitosis. Nat. Rev. Mol. Cell Biol. *14*, 549–562.
26. Andrews, N.W. (2000). Regulated secretion of conventional lysosomes. Trends Cell Biol. *10*, 316–321.
27. Medina, D.L., Fraldi, A., Bouche, V., Annunziata, F., Mansueto, G., Spampanato, C., Puri, C., Pignata, A., Martina, J.A., Sardiello, M., et al. (2011). Transcriptional Activation of Lysosomal Exocytosis Promotes Cellular Clearance. Dev. Cell *21*, 421–430.
28. Hubstenberger, A., Courel, M., Bénard, M., Souquere, S., Ernoult-Lange, M., Chouaib, R., Yi, Z., Morlot, J.B., Munier, A., Fradet, M., et al. (2017). P-Body Purification Reveals the Condensation of Repressed mRNA Regulons. Mol. Cell *68*, 144–157.e5.
29. Mizushima, N., Yamamoto, A., Matsui, M., Yoshimori, T., and Ohsumi, Y. (2004). In Vivo Analysis of Autophagy in Response to Nutrient Starvation Using Transgenic Mice Expressing a Fluorescent Autophagosome Marker. Mol. Biol. Cell *15*, 1101–1111.
30. Cormont, M., Mari, M., Galmiche, A., Hofman, P., and Le Marchand-Brustel, Y.L. (2001). A FYVE-finger-containing protein, Rabip4, is a Rab4 effector involved in early endosomal traffic. Proc. Natl. Acad. Sci. USA *98*, 1637–1642.
31. Mari, M., Macia, E., Le Marchand-Brustel, Y.L., and Cormont, M. (2001). Role of the FYVE Finger and the RUN Domain for the Subcellular Localization of Rabip4. J. Biol. Chem. *276*, 42501–42508.
32. Yang, J., Kim, O., Wu, J., and Qiu, Y. (2002). Interaction between Tyrosine Kinase Etk and a RUN Domain- and FYVE Domain-containing Protein RUFY1. A possible role of ETK in regulation of vesicle trafficking. J. Biol. Chem. *277*, 30219–30226.
33. Yamamoto, H., Koga, H., Katoh, Y., Takahashi, S., Nakayama, K., and Shin, H.W. (2010). Functional Cross-Talk between Rab14 and Rab4 through a Dual Effector, RUFY1/Rabip4. Mol. Biol. Cell *21*, 2746–2755.
34. Lu, Y., Wu, T., Gutman, O., Lu, H., Zhou, Q., Henis, Y.I., and Luo, K. (2020). Phase separation of TAZ compartmentalizes the transcription machinery to promote gene expression. Nat. Cell Biol. *22*, 453–464.
35. Yu, M., Peng, Z., Qin, M., Liu, Y., Wang, J., Zhang, C., Lin, J., Dong, T., Wang, L., Li, S., et al. (2021). Interferon-γ induces tumor resistance to anti-PD-1 immunotherapy by promoting YAP phase separation. Mol. Cell *81*, 1216–1230.e9.
36. Woodruff, J.B., Ferreira Gomes, B.F., Widlund, P.O., Mahamid, J., Honigmann, A., and Hyman, A.A. (2017). The Centrosome Is a Selective Condensate that Nucleates Microtubules by Concentrating Tubulin. Cell *169*, 1066–1077.e10.
37. Posey, A.E., Holehouse, A.S., and Pappu, R.V. (2018). Phase Separation of Intrinsically Disordered Proteins. Methods Enzymol. *611*, 1–30.
38. Choi, J.M., Holehouse, A.S., and Pappu, R.V. (2020). Physical Principles Underlying the Complex Biology of Intracellular Phase Transitions. Annu. Rev. Biophys. *49*, 107–133.

39. Terawaki, S., Camosseto, V., Prete, F., Wenger, T., Papadopoulos, A., Rondeau, C., Combes, A., Rodriguez Rodrigues, C., Vu Manh, T.P., Fallet, M., et al. (2015). RUN and FYVE domain-containing protein 4 enhances autophagy and lysosome tethering in response to Interleukin-4. J. Cell Biol. *210*, 1133–1152.

40. Clift, D., McEwan, W.A., Labzin, L.I., Konieczny, V., Mogessie, B., James, L.C., and Schuh, M. (2017). A Method for the Acute and Rapid Degradation of Endogenous Proteins. Cell *171*, 1692–1706.e18.

41. Banani, S.F., Lee, H.O., Hyman, A.A., and Rosen, M.K. (2017). Biomolecular condensates: organizers of cellular biochemistry. Nat. Rev. Mol. Cell Biol. *18*, 285–298.

42. Rawat, S., Chatterjee, D., Marwaha, R., Charak, G., Kumar, G., Shaw, S., Khatter, D., Sharma, S., de Heus, C., Liv, N., et al. (2023). RUFY1 binds Arl8b and mediates endosome-to-TGN CI-M6PR retrieval for cargo sorting to lysosomes. J. Cell Biol. *222*, e202108001.

43. Bowman, E.J., Siebers, A., and Altendorf, K. (1988). Bafilomycins: a class of inhibitors of membrane ATPases from microorganisms, animal cells, and plant cells. Proc. Natl. Acad. Sci. USA *85*, 7972–7976.

44. Klionsky, D.J., Abdel-Aziz, A.K., Abdelfatah, S., Abdellatif, M., Abdoli, A., Abel, S., Abeliovich, H., Abildgaard, M.H., Abudu, Y.P., Acevedo-Arozena, A., et al. (2021). Guidelines for the use and interpretation of assays for monitoring autophagy (4th edition). Autophagy *17*, 1–382.

45. Creasy, B.M., Hartmann, C.B., White, F.K., and McCoy, K.L. (2007). New assay using fluorogenic substrates and immunofluorescence staining to measure cysteine cathepsin activity in live cell subpopulations. Cytometry A *71*, 114–123.

46. Yoshida, H., Takakura, N., Kataoka, H., Kunisada, T., Okamura, H., and Nishikawa, S.I. (1997). Stepwise Requirement of c-kit Tyrosine Kinase in Mouse Ovarian Follicle Development. Dev. Biol. *184*, 122–137.

47. Lennartsson, J., Jelacic, T., Linnekin, D., and Shivakrupa, R. (2005). Normal and Oncogenic Forms of the Receptor Tyrosine Kinase Kit. Stem Cells *23*, 16–43.

48. Tziortzouda, P., Van Den Bosch, L.V.D., and Hirth, F. (2021). Triad of TDP43 control in neurodegeneration: autoregulation, localization and aggregation. Nat. Rev. Neurosci. *22*, 197–208.

49. Shin, S.W., Vogt, E.J., Jimenez-Movilla, M., Baibakov, B., and Dean, J. (2017). Cytoplasmic cleavage of DPPA3 is required for intracellular trafficking and cleavage-stage development in mice. Nat. Commun. *8*, 1643.

50. Scotter, E.L., Vance, C., Nishimura, A.L., Lee, Y.B., Chen, H.J., Urwin, H., Sardone, V., Mitchell, J.C., Rogelj, B., Rubinsztein, D.C., et al. (2014). Differential roles of the ubiquitin proteasome system and autophagy in the clearance of soluble and aggregated TDP-43 species. J. Cell Sci. *127*, 1263–1278.

51. Cheng, S., Altmeppen, G., So, C., Welp, L.M., Penir, S., Ruhwedel, T., Menelaou, K., Harasimov, K., Stützer, A., Blayney, M., et al. (2022). Mammalian oocytes store mRNAs in a mitochondria-associated membraneless compartment. Science *378*, eabq4835.

52. Li, L., Zhu, S., Shu, W., Guo, Y., Guan, Y., Zeng, J., Wang, H., Han, L., Zhang, J., Liu, X., et al. (2020). Characterization of Metabolic Patterns in Mouse Oocytes during Meiotic Maturation. Mol. Cell *80*, 525–540.e9.

53. Wan, Y., Yang, S., Li, T., Cai, Y., Wu, X., Zhang, M., Muhammad, T., Huang, T., Lv, Y., Chan, W.Y., et al. (2023). LSM14B is essential for oocyte meiotic maturation by regulating maternal mRNA storage and clearance. Nucleic Acids Res. *51*, 11652–11667.

54. Johnson, B.S., Snead, D., Lee, J.J., McCaffery, J.M., Shorter, J., and Gitler, A.D. (2009). TDP-43 Is Intrinsically Aggregation-prone, and Amyotrophic Lateral Sclerosis-linked Mutations Accelerate Aggregation and Increase Toxicity. J. Biol. Chem. *284*, 20329–20339.

55. Nie, X., Xu, Q., Xu, C., Chen, F., Wang, Q., Qin, D., Wang, R., Gao, Z., Lu, X., Yang, X., et al. (2023). Maternal TDP-43 interacts with RNA Pol II and regulates zygotic genome activation. Nat. Commun. *14*, 4275.

56. Miyazaki, Y., Mizumoto, K., Dey, G., Kudo, T., Perrino, J., Chen, L.C., Meyer, T., and Wandless, T.J. (2016). A method to rapidly create protein aggregates in living cells. Nat. Commun. *7*, 11689.

57. Moore, D.L., and Jessberger, S. (2017). Creating Age Asymmetry: Consequences of Inheriting Damaged Goods in Mammalian Cells. Trends Cell Biol. *27*, 82–92.

58. Rodríguez-Nuevo, A., Torres-Sanchez, A., Duran, J.M., De Guirior, C.D., Martínez-Zamora, M.A., and Böke, E. (2022). Oocytes maintain ROS-free mitochondrial metabolism by suppressing complex I. Nature *607*, 756–761.

59. Mindell, J.A. (2012). Lysosomal Acidification Mechanisms. Annu. Rev. Physiol. *74*, 69–86.

60. Finley, D. (2009). Recognition and Processing of Ubiquitin-Protein Conjugates by the Proteasome. Annu. Rev. Biochem. *78*, 477–513.

61. Mihalas, B.P., Redgrove, K.A., Bernstein, I.R., Robertson, M.J., McCluskey, A., Nixon, B., Holt, J.E., McLaughlin, E.A., and Sutherland, J.M. (2020). Dynamin 2-dependent endocytosis is essential for mouse oocyte development and fertility. FASEB J. *34*, 5162–5177.

62. Peters, A.E., Caban, S.J., McLaughlin, E.A., Roman, S.D., Bromfield, E.G., Nixon, B., and Sutherland, J.M. (2021). The Impact of Aging on Macroautophagy in the Pre-ovulatory Mouse Oocyte. Front. Cell Dev. Biol. *9*, 691826.

63. Jin, X., Wang, K., Wang, L., Liu, W., Zhang, C., Qiu, Y., Liu, W., Zhang, H., Zhang, D., Yang, Z., et al. (2022). RAB7 activity is required for the regulation of mitophagy in oocyte meiosis and oocyte quality control during ovarian aging. Autophagy *18*, 643–660.

64. Johnson, D.E., Ostrowski, P., Jaumouillé, V., and Grinstein, S. (2016). The position of lysosomes within the cell determines their luminal pHPosition. J. Cell Biol. *212*, 677–692.

65. Ratto, E., Chowdhury, S.R., Siefert, N.S., Schneider, M., Wittmann, M., Helm, D., and Palm, W. (2022). Direct control of lysosomal catabolic activity by mTORC1 through regulation of V-ATPase assembly. Nat. Commun. *13*, 4848.

66. Milovanovic, D., Wu, Y., Bian, X., and De Camilli, P.D. (2018). A liquid phase of synapsin and lipid vesicles. Science *361*, 604–607.

67. Bohnert, K.A., and Kenyon, C. (2017). A lysosomal switch triggers proteostasis renewal in the immortal C. elegans germ lineage. Nature *551*, 629–633.

68. Dhandapani, L., Salzer, M.C., Duran, J.M., Zaffagnini, G., De Guirior, C.D., Martínez-Zamora, M.A., and Böke, E. (2022). Comparative analysis of vertebrates reveals that mouse primordial oocytes do not contain a Balbiani body. J. Cell Sci. *135*.

69. Vitagliano, A., Paffoni, A., and Viganò, P. (2023). Does maternal age affect Assisted Reproduction Technology success rates after euploid embryo transfer? A systematic review and meta-analysis. Fertil. Steril. *120*, 251–265.

70. Chua, B.A., Lennan, C.J., Sunshine, M.J., Dreifke, D., Chawla, A., Bennett, E.J., and Signer, R.A.J. (2023). Hematopoietic stem cells preferentially traffic misfolded proteins to aggresomes and depend on aggrephagy to maintain protein homeostasis. Cell Stem Cell *30*, 460–472.e6.

71. Guo, Q., Lehmer, C., Martínez-Sánchez, A., Rudack, T., Beck, F., Hartmann, H., Pérez-Berlanga, M., Frottin, F., Hipp, M.S., Hartl, F.U., et al. (2018). In Situ Structure of Neuronal C9orf72 Poly-GA Aggregates Reveals Proteasome Recruitment. Cell *172*, 696–705.e12.

72. Terret, M.E., Wassmann, K., Waizenegger, I., Maro, B., Peters, J.M., and Verlhac, M.H. (2003). The Meiosis I-to-Meiosis II Transition in Mouse Oocytes Requires Separase Activity. Curr. Biol. *13*, 1797–1802.

73. So, C., Seres, K.B., Steyer, A.M., Mönnich, E., Clift, D., Pejkovska, A., Möbius, W., and Schuh, M. (2019). A liquid-like spindle domain promotes acentrosomal spindle assembly in mammalian oocytes. Science *364*, eaat9557.

74. Yeung, T., Gilbert, G.E., Shi, J., Silvius, J., Kapus, A., and Grinstein, S. (2008). Membrane Phosphatidylserine Regulates Surface Charge and Protein Localization. Science *319*, 210–213.

75. Schindelin, J., Arganda-Carreras, I., Frise, E., Kaynig, V., Longair, M., Pietzsch, T., Preibisch, S., Rueden, C., Saalfeld, S., Schmid, B., et al. (2012). Fiji: an open-source platform for biological-image analysis. Nat. Methods *9*, 676–682.

76. Mastronarde, D.N. (2005). Automated electron microscope tomography using robust prediction of specimen movements. J. Struct. Biol. *152*, 36–51.

77. Kremer, J.R., Mastronarde, D.N., and McIntosh, J.R. (1996). Computer Visualization of Three-Dimensional Image Data Using IMOD. J. Struct. Biol. *116*, 71–76.

78. Chiva, C., Olivella, R., Borràs, E., Espadas, G., Pastor, O., Solé, A., and Sabidó, E. (2018). QCloud: A cloud-based quality control system for mass spectrometry-based proteomics laboratories. PLoS One *13*, e0189209.

79. Perkins, D.N., Pappin, D.J.C., Creasy, D.M., and Cottrell, J.S. (1999). Probability-based protein identification by searching sequence databases using mass spectrometry data. Electrophoresis *20*, 3551–3567.

80. Vizcaíno, J.A., Csordas, A., del-Toro, N., Dianes, J.A., Griss, J., Lavidas, I., Mayer, G., Perez-Riverol, Y., Reisinger, F., Ternent, T., et al. (2016). 2016 update of the PRIDE database and its related tools. Nucleic Acids Res. *44*, D447–D456.

81. Kuma, A., and Mizushima, N. (2008). Chromosomal mapping of the GFP-LC3 transgene in GFP-LC3 mice. Autophagy *4*, 61–62.

82. Schuh, M., and Ellenberg, J. (2007). Self-Organization of MTOCs Replaces Centrosome Function during Acentrosomal Spindle Assembly in Live Mouse Oocytes. Cell *130*, 484–498.

83. Jaffe, L.A., and Terasaki, M. (2004). Quantitative Microinjection of Oocytes, Eggs, and Embryos. Methods Cell Biol. *74*, 219–242.

84. Clift, D., So, C., McEwan, W.A., James, L.C., and Schuh, M. (2018). Acute and rapid degradation of endogenous proteins by Trim-Away. Nat. Protoc. *13*, 2149–2175.

85. Thévenaz, P., Ruttimann, U.E., and Unser, M. (1998). A pyramid approach to subpixel registration based on intensity. IEEE Trans. Image Process. *7*, 27–41.

86. Carnell, M., Macmillan, A., and Whan, R. (2015). Fluorescence recovery after photobleaching (FRAP): acquisition, analysis, and applications. Methods Mol Biol. *1232*, 255–271.

87. Beer, L.A., Liu, P., Ky, B., Barnhart, K.T., and Speicher, D.W. (2017). Efficient Quantitative Comparisons of Plasma Proteomes Using Label-Free Analysis with MaxQuant. Methods Mol. Biol. *1619*, 339–352.

88. Bolte, S., and Cordelières, F.P. (2006). A guided tour into subcellular colocalization analysis in light microscopy. J. Microsc. *224*, 213–232.

89. Maekawa, M., and Fairn, G.D. (2014). Molecular probes to visualize the location, organization and dynamics of lipids. J. Cell Sci. *127*, 4801–4812.

90. Tapial, J., Ha, K.C.H., Sterne-Weiler, T., Gohr, A., Braunschweig, U., Hermoso-Pulido, A., Quesnel-Vallières, M., Permanyer, J., Sodaei, R., Marquez, Y., et al. (2017). An atlas of alternative splicing profiles and functional associations reveals new regulatory programs and genes that simultaneously express multiple major isoforms. Genome Res. *27*, 1759–1768.

91. Payer, B., Saitou, M., Barton, S.C., Thresher, R., Dixon, J.P.C., Zahn, D., Colledge, W.H., Carlton, M.B.L., Nakano, T., and Surani, M.A. (2003). stella Is a Maternal Effect Gene Required for Normal Early Development in Mice. Curr. Biol. *13*, 2110–2117.

92. Erdős, G., Pajkos, M., and Dosztányi, Z. (2021). IUPred3: prediction of protein disorder enhanced with unambiguous experimental annotation and visualization of evolutionary conservation. Nucleic Acids Res. *49*, W297–W303.

93. Jumper, J., Evans, R., Pritzel, A., Green, T., Figurnov, M., Ronneberger, O., Tunyasuvunakool, K., Bates, R., Žídek, A., Potapenko, A., et al. (2021). Highly accurate protein structure prediction with AlphaFold. Nature *596*, 583–589.

CellPress
OPEN ACCESS

STAR★METHODS

KEY RESOURCES TABLE

REAGENT or RESOURCE	SOURCE	IDENTIFIER
Antibodies		
Ms anti-ALIX	Abcam	Cat#ab117600; RRID: AB_10899268
Ms anti-EEA1	BD Bioscence	Cat#610456; RRID: AB_397829
Ms anti-PCNT	BD Biosciences	Cat#611815; RRID: AB_399295
Ms anti-Tubulin alpha (TUBA)	Sigma	Cat#T9026; RRID: AB_477593
Ms anti-Ubiquitin conjugates (FK2)	Merck Millipore	Cat#ST1200; RRID: AB_10681625
Rb anti-CANX	Abcam	Cat#ab22595; RRID: AB_2069006
Rb anti-CLTC	Abcam	Cat#ab21679; RRID: AB_2083165
Rb anti-CS	Abcam	Cat#ab96600; RRID: AB_10678258
Rb anti-DPPA3 (STELLAR)	Abcam	Cat#ab19878; RRID: AB_2246120
Rb anti-G3BP2	Abcam	Cat#ab86135; RRID: AB_1925011
Rb anti-GM130	ThermoFisher Scientific	Cat#PA5-95727; RRID: AB_2807529
Rb anti-HGS	Abcam	Cat#ab155539
Rb anti-LAMP1 [for oocytes]	Abcam	Cat#ab24170; RRID: AB_775978
Rb anti-LAMP1 [for HeLa cells]	Sigma	Cat#L1418; RRID: AB_477157
Rb anti-LC3B	Novus Biologicals	Cat#NB100-2220SS; RRID: AB_791015
Rb anti-LSM14B	Abcam	Cat#ab221041
Rb anti-MyoIIB	Abcam	Cat#ab230823
Rb anti-MyoVb	Novus Biologicals	Cat#NBP1-87746; RRID: AB_11034537
Rb anti-Proteasome 20S	Abcam	Cat#ab22673; RRID: AB_2268907
Rb anti-RUFY1	Proteintech	Cat#13498-1-AP; RRID: AB_2183747
Rb anti-TDP-43	Proteintech	Cat#10782-2-AP; RRID: AB_615042
Rb anti-Tubulin beta (TUBB)	Abcam	Cat#ab6046; RRID: AB_2210370
Rt anti-KIT (CD117)	BioLegend	Cat#105804; RRID: AB_313212
Rt anti-LAMP1 1D4B [for oocytes]	Abcam	Cat#ab25245; RRID: AB_449893
Gt anti-ZAR1	Santa Cruz Biotech	Cat#sc-55994; RRID: AB_2218783
Gt anti-Ms IgG (H+L), DyLight 680	ThermoFisher Scientific	Cat#35518; RRID: AB_614942
Gt anti-Ms IgG (H+L), Highly Cross-Adsorbed, Alexa Fluor 647	ThermoFisher Scientific	Cat#A-21236; RRID: AB_2535805
Gt anti-Rb IgG (H+L), Cross-Adsorbed, Alexa Fluor 555	ThermoFisher Scientific	Cat#A-21428; RRID: AB_2535849
Gt anti-Rb IgG (H+L), DyLight 800	ThermoFisher Scientific	Cat#SA5-35571; RRID: AB_2556775
Gt anti-Rb IgG (H+L), Highly Cross-Adsorbed, Alexa Fluor 647	ThermoFisher Scientific	Cat#A-21245; RRID: AB_2535813
Gt anti-Rt IgG (H+L), Cross-Adsorbed, Alexa Fluor 546	ThermoFisher Scientific	Cat#A-11081; RRID: AB_2534125
Gt anti-Rt IgG (H+L), Cross-Adsorbed, DyLight 680	ThermoFisher Scientific	Cat#SA5-10022; RRID: AB_2556602
Bacterial and virus strains		
E. coli NZY5α	NZYTECH	MB00402
Chemicals, peptides, and recombinant proteins		
Bafilomycin A1	Abcam	Cat#ab120497
Bovine Serum Albumin (BSA), heat-shock fraction	Sigma	Cat#A7906-500G

(*Continued on next page*)

Continued

REAGENT or RESOURCE	SOURCE	IDENTIFIER
Cytochalasin D	Sigma	Cat#C8273-10MG
DAPI	Sigma	Cat#D9542
Dibutyryladenosine-3′,5′-cyclic monophosphate (db-cAMP)	Sigma	Cat#D0627-250MG
DMEM	ThermoFisher	Cat#41965039
DMSO	Sigma	Cat#D2438-10ML
EmbryoMax advanced KSOM	MerckMillipore	Cat#MR-101-D
FM4-64FX	ThermoFisher	Cat#F34653
FOLIGON 6000U.I. (PMSG)	MSD Animal Health	Cat#2830 ESP
Hyaluronidase	Sigma	Cat#H4272-30MG
Leibovitz's L-15	Himedia	Cat#AT204-10X1
Lipofectamine	ThermoFisher	Cat#11668030
LysoTracker Deep Red	ThermoFisher	Cat#L12492
Magic Red Cathepsin B kit	Bio-Rad	Cat#ICT937
Me4BodipyFL-Ahx3Leu3VS	Bio-Techne	Cat#I-190-050
MG-132	MerckMillipore	Cat#474790-20MG
Mineral oil	Sigma	Cat#M8410-500ML
NidOil	Nidacon	Cat#NO-100
Nocodazole	Sigma	Cat#M1404-2MG
Normal Goat Serum (NGS)	Merck Millipore	Cat#S26-100ML
Phalloidin-Alexa488	ThermoFisher	Cat#A12379
Poly(vinyl alcohol), PVA	Sigma	Cat#P8136-250G
Proteostat	Enzo	Cat#ENZ-51035-K100
SiR-DNA	Tebu-bio	Cat#sc007
SPY555-Tubulin	Tebu-bio	Cat#sc203
SYBR Green	ThermoFisher	Cat#S7563
Vacuolin-1	Santa Cruz Biotech	Cat#sc-216045
VETERIN CORION 750U/ml (hCG)	DFV	Cat#2.006 ESP
Critical commercial assays		
First Strand cDNA synthesis kit	ThermoFisher	Cat#K1612
QIAquick PCR purification kit	QIAGEN	Cat#28104
mMessage mMachine SP6 kit	ThermoFisher	Cat#AM1340
Poly(A) tailing kit	ThermoFisher	Cat#AM1350
RNeasy MinElute RNA Cleanup kit	QIAGEN	Cat#74204
HiScribe T7 ARCA mRNA Kit (with tailing)	New England Biolabs	Cat#E2060S
RNeasy Mini Kit	ThermoFisher	Cat#74104
Deposited data		
Table S1	This paper	PRIDE: PXD042768, PXD047716
Table S2	This paper	PRIDE: PXD042769
Experimental models: Cell lines		
HeLa	ATCC	CCL-2; RRID: CVCL_0030
Experimental models: Organisms/strains		
C57BL/6J	Charles River	N/A
DBA/J	Charles River	N/A
B6CBAF1	In house	N/A
FvB/N	Janvier	N/A
CD1	Charles River	N/A

(*Continued on next page*)

CellPress
OPEN ACCESS

Continued

REAGENT or RESOURCE	SOURCE	IDENTIFIER
Tg(CAG-EGFP/Map1lc3b)53Nmz [GFP-LC3B Mouse]	Mizushima et al.[29]	MGI:3759813
Oligonucleotides		
See Table S4	This paper	N/A
Recombinant DNA		
pCS2-kozak-EGFP	This paper	N/A
pCS2-RUFY1-GFP FL	This paper	N/A
pCS2-RUFY1-GFP ΔIDR	This paper	N/A
pCS2-RUFY1-GFP ΔCC	This paper	N/A
pCS2-RUFY1-GFP ΔFYVE	This paper	N/A
pCS2-TDP-43(ΔNLS M337V)-GFP	This paper	N/A
AgDD-sfGFP	Miyazaki et al.[56]	Addgene Cat#78289
pCS2-AgDD-sfGFP	This paper	N/A
mCherry-RAB11A WT	Schuh, 2011[23]	N/A
mCherry-RAB11A S25N	Schuh, 2011[23]	N/A
pGEMHE-mTrim21	So et al.[73]	N/A
pGEMHE-mClover3-C1	Cheng et al.[51]	N/A
pGEMHE-mClover3-LACT-C2	This paper	N/A
LACT-C2-GFP	Yeung et al.[74]	Addgene Cat#22852
Software and algorithms		
ELVA calculator	This paper	Zenodo: https://doi.org/10.5281/zenodo.10446149
Prism 10	GraphPad	www.graphpad.com
FIJI	Schindelin et al.[75]	N/A
LAS X	Leica Microsystems	N/A
ZEN	Zeiss Group	N/A
SerialEM	Mastronarde et al.[76]	N/A
IMOD	Kremer et al.[77]	N/A
Proteome Discoverer v2.5	ThermoFisher	N/A
QCloud	Chiva et al.[78]	N/A
Mascot v2.6	Perkins et al.[79]	N/A

RESOURCE AVAILABILITY

Lead contact

Further information and requests for resources and reagents should be directed to and will be fulfilled by the lead contact, Elvan Böke (elvan.boke@crg.eu).

Materials availability

Plasmids generated in this study are available upon request to E.B. under a material transfer agreement with the Centre for Genomic Regulation (CRG).

Data and code availability

- The raw proteomics data have been deposited to the PRIDE repository[80] with the dataset identifiers PRIDE: PXD042768, PXD047716, and PXD042769, for Table S1, proteomics of GFP-LC3B FAPS-sorted ELVAs; Table S1, proteomics of FAPS-sorted ELVAs with alternative strategy; and Table S2, respectively.
- Scripts are available in Zenodo: https://doi.org/10.5281/zenodo.10446149 (ELVA Calculator macro for FIJI).
- Any additional information required to reanalyze the data reported in this paper is available from the lead contact upon request.

EXPERIMENTAL MODEL AND STUDY PARTICIPANT DETAILS

Mice

Oocytes were obtained from 8-to-12-weeks-old females. Eggs and embryos were obtained from superovulated 4-weeks-old females. For all experiments C57BL/6J mice were used, except where otherwise specified. For the experiments shown in Figures 7A, 7B, and S6A B6CBAF1 mice were used. For TRIM-Away FvB/N mice were used. C57BL/6J, CBA/J and CD1 mice were purchased from Charles River Laboratories, FvB/N mice from Janvier. B6CBAF1 mice were obtained crossing CBA/J males with C57BL/6J females. GFP-LC3B mice[29] were obtained from Pura Muñoz Canoves (UPF, Barcelona), backcrossed to C57BL/6J and bred to homozygosity. Genotyping was performed as previously described.[81] All mice were housed in individually-ventilated cages at 22°C with 12h light/darkness cycles in specific pathogen-free conditions and fed *ad libitum* according to the Federation of European Laboratory Animal Science Association guidelines and recommendations. Animal handling was performed by accredited personnel. The animal husbandry and superovulation procedures were approved by the local ethical committee (Comité Ético de Experimentación Animal del PRBB (CEEA-PRBB), and met the guidelines of the local and European regulations.

Cell lines

HeLa cells (CCL-2- ATCC), female, were grown in a humidified incubator at 37°C 5% CO_2 in DMEM (ThermoFisher, 41965039) supplemented with 1mM sodium pyruvate (ThermoFisher, 11360070) and 10% Fetal Calf Serum (ThermoFisher, 10270106). Cultures were tested routinely for mycoplasma infection.

Bacterial Strains

Plasmids were amplified in *E. coli* NZY5α. Cells were grown in LB with appropriate antibiotics at 37°C.

METHOD DETAILS

Oocytes, eggs and embryo collection and culture

All isolations were performed at 37°C on a dissection microscope equipped with a heated stage plate (Tokai Hit). Maturation-incompetent (NSN) and -competent (SN) oocytes were collected from the ovaries of unstimulated young adult mice (8-12 weeks). Ovaries were collected in homemade M2 and punctured with 30G needles. Oocytes were collected in M2 supplemented with 200μM dibutyryl cyclic AMP (db-cAMP) using an 80μm-bore Flexipet (Cook), and denuded by repeated pipetting. For *in vitro* maturation oocytes were incubated at 37°C for at least 30', then only oocytes showing perivitelline space (PVS) were selected, transferred to M2 without db-cAMP and incubated at 37°C for ~14h. Ovulated eggs were collected from 4-weeks old females injected intraperitoneally with 7.5-10U pregnant mare's serum gonadotropin (PMSG) followed by 7.5-10U human chorionic gonadotropin (hCG) 48-50h apart. Cumulus-oocyte complexes were collected 13-14h after hCG injection in M2 supplemented with 250U Hyaluronidase, and isolated eggs were transferred to fresh M2. For 1-cell embryos collection, mice were superovulated as described and mated 1:1 with individualized males immediately after hCG injection. Embryos were retrieved from plug-positive females 22-24h after hCG injection in M2 supplemented with Hyaluronidase, and 1-cell embryos with two visible pronuclei (2PN) were collected. For preimplantation embryo development, embryos were cultured in EmbryoMAX advanced KSOM at 37°C 5% CO_2 for up to 4 overnights. For all experiments, oocytes, eggs and embryos were retrieved from multiple animals and pooled together. Where applicable, oocytes/embryos were randomly distributed to the different experimental conditions.

Drugs, dyes and other live treatments

For FM4-64FX labelling, oocytes were loaded with 5μM FM4-64FX for 3-4h in M2 + db-cAMP at 37°C, then washed in fresh M2 to allow maturation. Oocytes injected with RUFY1-GFP mutants and loaded with FM4-64FX were imaged in M2 + db-cAMP to prevent meiosis resumption. For Lysotracker Deep Red labelling oocytes were incubated with 50nM LysoTracker for at least 45-60min before imaging. Magic Red Cathepsin B was resuspended following manufacturer's instruction and used 1:2000. For Bafilomycin A1 (BafA1) treatment oocytes were pre-incubated with or without 250nM BafA1 for 1-2h at 37°C in M2 + db-cAMP before allowing maturation in M2 +- 250nM BafA1. For CytochalasinD (CytoD) and Nocodazole (Noco) treatments, oocytes were matured overnight in presence of 1μg/ml CytoD ad 5μg/ml Noco in M2. For Me4BodipyFL labelling oocytes were incubated for 1h at 37°C with 500nM dye before imaging. MG-132 was used at 10μM final, oocytes were preincubated with MG-132 for 1-2h in M2 + db-cAMP, then labelled with Me4BodipyFL or transferred to fresh M2 + MG-132 to allow maturation and then labelled with Me4BodipyFL. SiR-DNA, SPY555-Tubulin were resuspended according to the manufacturer's instructions and used 1:1000. Vacuolin-1 was used at 5μM final. For all drug treatments an equivalent amount of DMSO was added to the control sample (1:1000 or less). DMSO was taken with a syringe from an air-tight bottle immediately prior to use.

The choice of markers to label ELVAs (LAMP1 or RUFY1) was performed mostly due to antibody availability for colocalization experiments. For live markers used to image ELVAs (FM4-64 and GFP-LC3 transgenic oocytes), the choice of both live markers allowed us to image ELVAs in combination with different live-cell probes (Me4BodipyFL and Lysotracker Deep Red) that would otherwise not be spectrally compatible with either marker.

Mouse oocyte cDNA library preparation

~600 oocytes were collected, washed 2x2mL in L-15 0.01% PVA and collected in ~50μl in a tube, then spun at 50g for 15s RT. The supernatant was carefully removed and the pellet diluted in 500μl TRI Reagent (Sigma, T9424) and vortexed, then supplemented with 100μL chloroform, vortexed vigorously, and incubated at RT for 5min, then centrifuged at 20800g for 15min at 4°C. The upper phase was collected and supplemented with 250μl Isopropanol + 40μg/ml final Linear acrylamide (ThermoFisher, AM9520), vortexed, incubated on ice for 5min and spun at 20800g for 30min at 4°C. The pellet was gently washed in 1ml 75% ethanol 25% DEPC water, spun for 5min at 20000g at 4°C and the supernatant was carefully removed. The pellet was resuspended in 20μl DEPC water, quantified with nanodrop, and stored at -80°C. ~800ng RNA were retro-transcribed with First Strand cDNA synthesis kit (ThermoFisher scientific, K1612) with oligo-dT following the manufacturer's instructions.

DNA Constructs

RUFY1 was amplified from a mouse oocyte cDNA library and cloned into pCS2-kozak-EGFP via EcoRI and BamHI at the N-terminus of EGFP, to generate pCS2-RUFY1-GFP. N- and C-terminal deletions of RUFY1 were amplified from pCS2-RUFY1-GFP and cloned into empty pCS2-kozak-EGFP via EcoRI and BamHI. Internal RUFY1 deletions were generated via PCR-based mutagenesis using divergent primers on the pCS2-RUFY1-GFP template. TDP-43 M337V ΔNLS was a kind gift of Anthony Hyman (MPI-CBG, Dresden) and was subcloned into pCS2-EGFP via Gibson Assembly to generate TDP-43-GFP M337V ΔNLS. AgDD-GFP was purchased from Addgene (plasmid n. 78289) and subcloned into pCS2 via Gibson Assembly for *in vitro* transcription. The full coding sequence of all constructs was sequenced for confirmation. mCherry-RAB11A WT and S25N constructs have been previously described.[23] pGEMHE-mTrim21 for TrimAway was also previously described.[73] For pGEMHE-mClover3-LACT-C2 construction LACT-C2 was amplified from LACT-C2-GFP (Addgene Plasmid #22852)[74] and fused with XhoI- and BamHI-digested pGEMHE-mClover3-C1[51] via Gibson Assembly. The PCR primers used for cloning and sequencing the constructs are listed in Table S4.

In vitro transcription and mRNA injection

pCS2-RUFY1-GFP, pCS2-TDP-43-GFP M337V ΔNLS and pC2-AgDD-GFP constructs were linearized o/n at 37°C, purified with QIAquick PCR purification kit (QIAGEN, 28104) and eluted with RNAse-free water. ~1μg linearized DNA was *in vitro* transcribed with mMessage mMachine SP6 kit (ThermoFisher scientific, AM1340) for 2h at 37°C. RNAs were polyadenylated with Poly(A) tailing kit (ThermoFisher scientific, AM1350) for 1h at 37°C, purified with RNeasy MinElute RNA Cleanup kit (QIAGEN, 74204), eluted in RNAse-free water, quantified and the concentration adjusted to 1μg/μl. All RNA batches were run in a 0.8% agarose gel before injection to validate correctness and integrity of the transcripts. mRNAs were filtered through an Ultrafree MC centrifugal filter (Millipore) and injected in the cytoplasm of GV-stage oocytes or 1-cell embryos maintained in M2 (+-db-cAMP, respectively) at 37°C using Femtotip II injection needles (Eppendorf) and a FemtoJet microinjector (Eppendorf). All injected oocytes were incubated at 37°C in M2 + db-cAMP for 3-5h before imaging. Injected embryos were washed in KSOM and incubated overnight in KSOM at 37°C 5% CO2. mClover-LACT-C2, mCherry-RAB11A WT and S25N and mTrim21 mRNAs were synthesized using the HiScribe T7 ARCA mRNA Kit (with tailing) (New England Biolabs, E2060S) and purified with RNeasy Mini Kit (QIAGEN, 74104). Mouse oocytes were microinjected with 6 pl of mRNAs as previously described.[82,83] mClover3-LACT-C2 mRNA was injected at a concentration of 0.3μM in the injection solution. mCherry-RAB11A and mCherry-RAB11A(S25N) were both injected at a concentration of 0.5μM. All injected oocytes were incubated at 37°C in M2 + db-cAMP for 4-5h before imaging.

Trim-Away

2pl of mRNA mixture containing 0.5μM mTrim21, with or without 0.3μM mScarlet-LACT-C2, were co-injected with 4pl of anti-RUFY1 antibody at 1mg/ml or normal rabbit IgG (Merck Millipore, 12-370) supplemented with 0.1% NP-40 as previously described.[40,84] Oocytes were incubated in homemade phenol red–free M2 medium supplemented with 250μM db-cAMP for 4-6h before imaging or fixation.

Live imaging of oocytes

Oocytes were placed in small M2 droplets on a glass-bottom 35mm dish (MatTek, P35G-1.5-20-C) covered with NidOil (Nidacon) and imaged with a confocal microscope (Leica TCS SP5II) at 37°C using a 20x or 63x glycerol-immersion lens. For live imaging of oocyte maturation oocytes were imaged for 13-15h with time points every 5-15minutes. For all oocytes, stacks were taken encompassing the entire oocyte with slices every 2-3μm. mCherry-RAB11A and mClover-LACT-C2-injected oocytes were imaged an LSM880 confocal laser scanning microscope (Zeiss) equipped with an environmental incubator box and a 40× C-Apochromat 1.2N.A. water-immersion objective.

FRAP

For FRAP on RUFY1-GFP-labelled ELVAs in live oocytes, on average only the 2-3 ELVAs per oocyte were bleached (typically the largest ones). A circular ROI was drawn in the center of each ELVA and bleached with maximal 488nm laser power after 2-3 time points. ELVAs were recorded for 1-3 minutes with time points every 1-3s. For quantification the stacks were registered in FIJI with the StackReg plugin using the "Translation" option,[85] then the average intensity of a ROI corresponding to the bleached area was measured in all slices as a readout. For each track, all data points were normalized on the last time point before bleaching.

To calculate the recovery halftimes ($t_{1/2}$) and mobile fractions (F_m) data were fitted to monoexponential curves (R^2>0.99 for all curves), F_m were then calculated as follows: $F_m = (I_{pl} - I_0) / (I_{pre} - I_0)$, where I_{pl} is the fluorescence intensity at plateau, I_0 is the intensity at t=0 (first time point after bleaching) and I_{pre} is the pre-bleaching intensity.[86]

Transfection and imaging of cultured cells

Plasmid transfections were performed using lipofectamine 2000 (ThermoFisher, 11668030) following the recommended protocol. For a 35mm plate 4μg plasmid and 10μl lipofectamine 2000 were used. After 6h transfection, the transfection medium was replaced with fresh DMEM and cells were incubated at 37C 5% CO_2 for 18-24h. Transfected cells were fixed for immunofluorescence or further incubated with SiR-DNA 1:1000 for at least 30min before imaging, then imaged live at 37C 5% CO_2 with a Leica TCS SP5II confocal microscope equipped with a 63x oil-immersion lens.

Immunofluorescence of oocytes and embryos

Oocytes and embryos were fixed for 1h RT in 2% formaldehyde in PBS supplemented with 0.05% BSA to prevent adhesion to the plastic. Cells were permeabilized in PBS 0.05% Triton X100 for 30min RT, blocked for 1hr RT in PBS 3% BSA 1% Normal Goat Serum (NGS) 0.1% Tween20 and incubated o/n in blocking with primary antibodies. Cells were washed for 1h RT in blocking, incubated for 1.5-2h RT in blocking with Alexa-conjugated secondary Antibodies, washed for 1h in blocking, rinsed in PBS 0.05% BSA and placed in small droplets of PBS on a glass-bottom 35mm dish (MatTek) covered with mineral oil. Imaging was performed with a confocal microscope (Leica TCS SP5 or SP8) equipped with a 40x or 63x water immersion lens. DNA was counterstained with DAPI. For the LAMP1 immunostaining shown in Figure S6B cells were permeabilized with 0.1% Tween20 for 1hr RT instead than Triton X100, to allow optimal detection of free lysosomal puncta. For Proteostat staining, oocytes and embryos were processed following the manufacturer's instructions: cells were fixed with 2% formaldehyde in 1X Assay Buffer 0.05% BSA for 1hr RT, permeabilized in 1X Assay Buffer 0.5% Triton X100 3mM EDTA for 1h on ice, washed in PBS 0.05% BSA, immunolabelled with primary antibodies for 1h RT in 1X Assay Buffer 0.05% BSA, washed in PBS 0.05% BSA for 1hr RT, incubated with secondary antibodies + Proteostat 1:2000 for 1h RT in 1X Assay Buffer 0.05% BSA, washed in PBS 0.05% BSA and spotted for imaging as described. DNA was counterstained with Hoechst 33342, provided in the kit.

For spindle immunolabelling with anti-Tubulin and anti-Pericentrin (PCNT), F-Actin staining and Ubiquitin conjugates immunolabeling upon BafA1 treatment, oocytes were fixed and labelled as previously described.[82] Briefly, oocytes were fixed in 2% formaldehyde in 100mM Hepes, 50mM EGTA, 10mM $MgSO_4$, 0.2% Triton X100 pH 7.0 (adjusted with KOH) for 1h at 37C, then extracted in PBS 0.1% Triton X100 overnight at 4C. Oocytes were incubated with primary antibodies for 2h RT in PBS 0.1% Triton X100 3% BSA 1% NGS (PBT), washed in PBT for 1h RT, incubated with secondary antibodies for 1.5h RT in PBT, washed for 1h in PBT, rinsed in PBS and spotted for imaging as described above.

For LC3B immunofluorescence oocytes were fixed in 70% methanol 30% acetic acid for 20min at -20C, washed in PBS 0.1% saponin and blocked for 1hr RT in PBS 0.1% saponin 3% BSA 1% NGS, then incubated o/n at 4C in blocking with primary antibodies. Oocytes were washed for 1hr RT in PBS 0.1% saponin, incubated for 2h RT in blocking with secondary antibodies, washed for 1hr RT in PBS 0.1% saponin and spotted for imaging as described.

For immunolabeling of unpermeabilized oocytes and embryos, cells were fixed in 2% FA 0.05% BSA in PBS for 1hr RT, blocked in PBS 3% BSA 1% NGS for 45min RT, incubated with Rt aLAMP1 1D4B (Abcam) in blocking for 45min RT, washed for 30min RT in blocking, incubated in blocking with secondary antibody for 45min RT, washed for 45min in PBS 0.05% BSA and spotted for imaging as described. The DNA was counterstained with SybrGreen.

For immunofluorescence after Trim-Away oocytes were fixed 6-16h after db-cAMP washout with 4% methanol-free formaldehyde in PBS for 1 hour at room temperature. Fixed oocytes were washed and extracted with PBT buffer (0.5% Triton X-100 in PBS) for 1 hour at room temperature or overnight at 4°C. Permeabilized oocytes were blocked with PBT-BSA buffer (PBS 3% BSA 0.1% Triton X-100) for 1 hour at room temperature or overnight at 4°C. Oocytes were incubated with primary antibodies in PBT-BSA for 1.5 hours at room temperature. After washing three times with PBT-BSA, oocytes were incubated with secondary antibodies and Hoechst 33342 (ThermoFisher Scientific, H3570) for 1.5 hours at room temperature. Oocytes were washed three times and imaged in 2-3μl of PBS supplemented with 10% fetal bovine serum (Gibco, 16000-044) under paraffin oil in a 35-mm dish with a No. 1.0 coverslip using a LSM880 laser confocal microscope (Zeiss). For all experiments, primary antibodies were used 1:50 – 1:100, except anti-RUFY1 (1:300). Secondary antibodies were used 1:100.

Immunofluorescence of cultured cells

Transfected HeLa cells were fixed in 4% methanol-free formaldehyde in 100mM phosphate buffer pH 7.4 for 15min RT, permeabilized in PBS 0.5% Triton X100 for 15min RT, blocked for 30min RT in PBS 3% BSA 1% Normal Goat Serum 0.1% saponin and incubated with primary antibodies 1:100 overnight in blocking buffer at 4C. Cells were washed 3x10min in PBS, incubated with secondary antibodies 1:500 in blocking for 1hr at 4C, washed in PBS and mounted. For LC3B immunolabelling, cells were fixed in 100% methanol for 5min at -20C, then immediately blocked and immunolabelled as described.

Immunohistochemistry

Young adult mouse ovaries were fixed in 4% formaldehyde in PBS overnight at 4°C, washed, embedded in paraffin blocks and cut into 5μm-thick sections. After deparaffinization, antigen retrieval was performed by boiling the slides in 10 mM sodium citrate at pH 6.0. Sections were blocked in 3% BSA, 0.05% Tween-20 and 0.05% Triton X-100 for 1 h at room temperature, then incubated overnight at 4 °C in blocking with primary antibodies (1:100). Sections were washed for 1hr RT in blocking, then incubated for 2h RT in blocking with secondary antibodies (1:100), washed for 30min RT in blocking, rinsed in PBS and mounted with Fluorshield with DAPI (Sigma, F6057-20ML). Sections were imaged with a Leica TCS SP5 confocal microscope equipped with 40x or 63x oil-immersion lens. For immunohistochemistry with anti-CLTC, ovaries were fixed in Methacarn (60% methanol, 30% chloroform, 10% acetic acid) o/n at 4°C, then embedded into paraffin and cut into 5μm-thick sections. After deparaffinization sections were treated with 0.05% trypsin in 10mM CaCl2 for 5min at 37°C for antigen retrieval, then rinsed thoroughly with distilled water. Immunolabelling was performed as described as above. For Proteostat labelling of mouse ovarian sections, formaldehyde-fixed, paraffin-embedded slides were de-paraffinized and incubated in 1x Assay Buffer 0.5% Triton X100 3mM EDTA on ice for 1h. Slides were washed in PBS and incubated for 1h in 1X Assay buffer with primary antibody 1:100 at RT. Slides were washed for 1h RT in PBS, incubated for 1h at RT in 1x Assay Buffer with Secondary Antibody 1:100 + Proteostat 1:2000, washed for 1h RT in PBS and mounted.

Electron microscopy

Conventional Transmission Electron Microscopy

Mouse oocytes, eggs and embryos were fixed and shipped at RT in 2% methanol-free formaldehyde (FA) 1% glutaraldehyde (GA, Electron Microscopy Sciences, 16100) in PBS or in 4% FA, 0.05% GA in PBS and post-fixed in 1% GA in PBS for 10 min. Samples were washed in PBS and contrasted with 1% reduced osmium tetroxide (OsO4, EMS), 1.5% potassium ferrocyanide (Sigma) for 1h at 4°C. Samples were washed with ultrapure water at least three times between each step. Staining was enhanced by incubation with 0.2% tannic acid (EMS) for 10min at room temperature. A further contrasting step with 0.5% uranyl acetate (EMS) in 35% methanol was performed overnight at 4°C. The tissue was gradually dehydrated with increasing concentrations of ethanol (starting at 30%), followed by a stepwise infiltration with epoxy resin (EMBed812, EMS). A final infiltration step in pure resin was performed at least overnight. The resin was finally cured at 60°C for at least 24hrs. For conventional TEM analysis, 70nm-thick sections were cut on a Leica UCT ultramicrotome (Leica Microsystems, Wetzlar, Germany) onto formvar-coated slot grids and post-stained with 2% aqueous uranyl acetate and 0.04% aqueous lead citrate (EMS). Sections were analyzed with a Morgagni TEM (FEI) at 80KV equipped with a Morada CCD camera and ITEM software (EMSIS, Münster, Germany). For TEM tomography, 300nm-thick sections were cut on a Leica UCT microtome on formvar-coated slot grids and post-stained with 1% uranyl acetate in 70% methanol and 0.04% aqueous lead citrate. 15nm colloidal gold particles as fiducial markers were applied on both section sides. Tomograms were acquired at 300KV on a Tecnai F30 TEM (Thermofisher/FEI) equipped with a OneView camera (Gatan). SerialEM[76] was used for automatic acquisition of the tomograms at dual-tilt with +/-64° with 1° steps. The tomograms were reconstructed into virtual stack slices using the IMOD software package.[77]

Immuno-correlative Light Electron Microscopy

Mouse oocytes were fixed in 4% FA, 0.01% GA in PBS, washed twice with PBS and quenched with 0.1% glycine in PBS for 5 min. Oocytes were rinsed with PBS and transferred into droplets of 12% gelatin in PBS at 37°C. Gelatin was solidified at 4°C for 1h, then small cubes containing the oocytes were cut and infiltrated in 2.3M sucrose in PBS overnight. Blocks were mounted on aluminum pins and snap-frozen in liquid nitrogen. Tokuyasu cryo-sections were cut on a Leica UC7 ultramicrotome (Leica Microsystems). Sections were picked and transferred onto formvar-coated mesh grids with a combination of 1% methyl cellulose (Sigma) and 1.1M sucrose. Sections were stored at 4°C until immunolabelling. For immunolabelling, gelatin was removed by floating the sections on PBS at 37°C for 45min. Sections were blocked on droplets of 0.5% BSA, 0.2% gelatin in PBS (blocking buffer) for 2x10min. Sections were labelled in blocking buffer with Rb anti-LAMP1 1:30 for an hour, washed in blocking buffer and labelled in blocking buffer with 10nm gold-conjugated goat anti-Rb IgG 1:30 (British Biocell). Sections were washed and further labelled with Alexa594-conjugated donkey anti-Rb IgG 1:200 (Molecular Probes) in PBS, washed in PBS and mounted in Vectashield (Vectorlabs) on a glass slide, then imaged with an upright epifluorescence ApoTome microscope equipped with an Axiocam506 camera (Zeiss). After fluorescent imaging, the grids were thoroughly rinsed in water and contrasted with a mixture of 1.9% methyl cellulose and 0.3% uranyl acetate for 10min on ice. Grids were imaged using a Morgagni TEM (FEI) with Morada CCD camera and ITEM software (EMSIS). Images were analyzed in Fiji.

FAPS

~300 GFP-LC3B or WT isolated oocytes per experiment were denuded thoroughly by mechanical pipetting as described, washed in L-15 0.05% PVA, treated with homemade Acid Tyrode's Solution supplemented with 0.05% PVA to remove the Zona Pellucida, collected in PBS 0.05% PVA and lysed in a 100μl-volume drop of PBS supplemented with cOmplete EDTA-free protease inhibitors (Roche, 4693132001) in a 35mm Petri dish. Lysis was performed pipetting zona-free oocytes with an 80μm-bore Flexipet (Cook) with the tip flattened by gentle squeezing with a flat object against the bench surface. Oocytes were processed in small groups in order to minimize the incubation times in Tyrode's solution and PBS before lysis. Lysed oocytes were diluted 1:1 with lysis buffer, supplemented with SiR-DNA 1:100 to label residual intact granulosa cells, and filtered through a 35μm-bore cell strainer to remove large debris. Lysates were kept on ice until FAPS sorting. Sorting was performed with a FACS Aria II (BD Biosciences) instrument using a 100μm nozzle and the BD FACS flow sheath fluid (BD Biosciences, 342003) at 4°C. GFP-positive events from GFP-LC3B oocyte

lysates were gated based on the fluorescence of WT lysates and sorted directly into a 1.5ml Eppendorf tube placed at 4°C. For the alternative FAPS strategy, WT C57BL/6J oocytes were isolated and loaded with anti-KIT-biotin (Biolegend) + Streptavidin-Alexa488 (ThermoFisher), FM4-64FX or both for 3h at 37°C, then treated and lysed as described. 10% of the lysates was saved as input for the proteomics experiment. Anti-KIT-488 and FM-4-64 were detected with FITC and PerCP-Cy5.5 filters, respectively.

Mass Spectrometry

Sample preparation

FAPS-sorted samples were spun for 15min at 20000g at 4°C, the supernatant was carefully removed, and the pellet was resuspended in 10μl 6M guanidinium chloride in 10mM EPPS pH 8.5. For mass spectrometry of oocytes treated with or without BafA1 during maturation, the same amount of MII eggs per condition (~100 per experiment) was washed in L-15 0.01% PVA, treated with Acid Tyrode'sSolution 0.01% PVA to remove the Zona Pellucida and collected in 1μl L-15 0.01% PVA, then diluted with 20μl 6M guanidinium chloride in 10mM EPPS pH 8.5. Samples were heated at 60°C for 30min, diluted with EPPS pH 8.5 to 2M Guanidinium chloride and digested with LysC (10 ng/μl) overnight at RT. Samples were further diluted to 0.5M Guanidinium chloride and digested with LysC (10 ng/μl) and trypsin (5ng/μl) for further 8h at 37°C. Samples were acidified with formic acid to a final concentration of 10% and desalted with home-made C18 columns. Columns were equilibrated with 100% acetonitrile, then 70% acetonitrile 30% 1% formic acid in milliQ water, 30% acetonitrile 70% 1% formic acid, and finally 100% 1% formic acid. For all steps 30μl were loaded and spun at 2000g for 10min or until columns were empty. Samples were applied to equilibrated columns and spun at 2000g until empty. Columns were washed 2x100μl with 1% Formic Acid and peptides eluted with 20μl 30% Acetonitrile 70% 1% Formic Acid, then with 20μl 70% Acetonitrile 30% 1% Formic Acid. Eluates were pooled and stored at -20°C until processing for LC-MS.

Chromatographic and mass spectrometric analysis

Samples were analyzed using a Orbitrap Eclipse mass spectrometer (Thermo Fisher Scientific, San Jose, CA, USA) coupled to an EASY-nLC 1200 (Thermo Fisher Scientific (Proxeon), Odense, Denmark). Peptides were loaded directly onto the analytical column and were separated by reversed-phase chromatography using a 50-cm column with an inner diameter of 75μm, packed with 2μm C18 particles spectrometer (Thermo Scientific, San Jose, CA, USA). Chromatographic gradients started at 95% buffer A (0.1% formic acid in water) and 5% buffer B (0.1% formic acid in 80% acetonitrile) with a flow rate of 300 nl/min and gradually increased to 25% buffer B and 75% A in 79 min and then to 40% buffer B and 60% A in 11 min. After each analysis, the column was washed for 10 min with 100% buffer B. The mass spectrometer was operated in positive ionization mode with nanospray voltage set at 2.4 kV and source temperature at 305°C. The acquisition was performed in data-dependent acquisition (DDA) mode and full MS scans with 1 micro scans at resolution of 120,000 were used over a mass range of m/z 350-1400 with detection in the Orbitrap mass analyzer. Auto gain control (AGC) was set to 'standard' and injection time to 'auto'. In each cycle of data-dependent acquisition analysis, following each survey scan, the most intense ions above a threshold ion count of 10000 were selected for fragmentation. The number of selected precursor ions for fragmentation was determined by the "Top Speed" acquisition algorithm and a dynamic exclusion of 60 seconds. Fragment ion spectra were produced via high-energy collision dissociation (HCD) at normalized collision energy of 28% and they were acquired in the ion trap mass analyzer. AGC was set to 2E4, and an isolation window of 0.7 m/z and a maximum injection time of 12ms were used. Digested bovine serum albumin (New England Biolabs, P8108S) was analyzed between each sample to avoid sample carryover and to assure stability of the instrument and QCloud[78] was used to control instrument longitudinal performance during the project.

Data analysis

Acquired spectra were analyzed using the Proteome Discoverer software suite (v2.0, Thermo Fisher Scientific) and the Mascot search engine (v2.6, Matrix Science[79]). The data were searched against a Swiss-Prot mouse database plus a list[87] of common contaminants and all the corresponding decoy entries. For peptide identification a precursor ion mass tolerance of 7ppm was used for MS1 level, trypsin was chosen as enzyme, and up to three missed cleavages were allowed. The fragment ion mass tolerance was set to 0.5 Da for MS2 spectra. Oxidation of methionine and N-terminal protein acetylation were used as variable modifications whereas carbamidomethylation on cysteines was set as a fixed modification. False discovery rate (FDR) in peptide identification was set to a maximum of 5%. Peptide quantification data were retrieved from the "Precursor ion area detector" node from Proteome Discoverer (v2.3 or 2.5) using 2ppm mass tolerance for the peptide extracted ion current (XIC). The obtained values were used to calculate protein fold-changes and their corresponding adjusted p-values.

For all experiments, only proteins with >1 unique peptides were considered for further analysis. For mass-spectrometry of GFP-LC3B FAPS-sorted ELVAs, proteins shared between the two replicates are listed in Table S1. For proteomics of FAPS-sorted ELVAs with the alternative sorting strategy, proteins with at least 2 unique peptides enriched at least 5 times in double-labelled sample with respect to single-labelled controls are listed. Proteins with mitochondrial localization were removed due to mitochondrial autofluorescence. For mass spectrometry of *in vitro* matured oocytes in presence or absence of BafA1, only proteins with an abundance value in both samples were considered. Each value was normalized against the total abundance of the respective sample, then the ratio BafA1/DMSO for each protein was calculated. For the three replicates the BafA1/DMSO ratios of total protein amounts were 1.24, 0.92 and 1.08, respectively.

Western Blotting

~60 isolated oocytes were washed 2x in Leibovitz's L-15 + 0.005% Poly-vinyl alcohol (PVA), collected in 1μl L-15 PVA and diluted with 10μl 1X Sample Buffer. For NIH 3T3 a 35mm plate at confluency was trypsinized, counted, spun at 200g for 5min RT, washed in PBS and resuspended in 1X Sample Buffer at a final concentration of ~1000 cells/μl. The whole oocyte lysate and the equivalent of ~20000 3T3 cells were boiled at 70C for 5min, run in a 4-12% Bis Tris NuPage polyacrylamide gel in MOPS at 150V, transferred on a 0.45μm-pore size PVDF membrane in 20% Methanol at 100V for 2h on ice, blocked for 30min in Odyssey® Blocking Buffer in PBS (Licor, 927-40000) and incubated o/n at 4C in blocking with primary antibodies 1:1000. Membranes were washed for 30min in PBS 0.1% Tween20 (PBST), incubated for 2h RT in blocking with secondary antibodies 1:1000, washed for 30 min in PBST, rinsed in PBS and imaged with a Licor Odyssey DLx imager.

QUANTIFICATION AND STATISTICAL ANALYSIS

ELVA number, size and position were quantified with a custom-made FIJI macro, available in Zenodo: https://doi.org/10.5281/zenodo.10446149. All quantifications relied on object segmentation based on the 3D object counter plugin.[88] ELVAs were segmented as objects larger than 100 voxels (~8μm^3 volume). The goodness of object picking was assessed for all oocytes overlaying the masks of segmented objects to the raw images. The radius of each ELVA was extrapolated from the respective volume, assuming sphericity. Examples and comparison with manual quantification are provided in Figures S2A–S2C. For manual quantification, ELVAs were segmented in FIJI with the magic wand with tolerance 30-50. For ELVAs encompassing multiple slices, only the equatorial slice was considered. The radius of individual ELVAs was calculated as the average between the major and minor axis of the best fitting ellipse ("Set measurements" -> "Fit ellipse").

For quantification of ELVA distance from the cortex the centroid of each automatically segmented ELVA was overlaid to a distance map of the oocyte boundaries in the corresponding z-slice (Figure S2A), and the corresponding distance value was taken as readout. For measuring the mean intensity of dyes and proteins inside ELVAs, automated ELVA segmentation was performed as described on a separate channel displaying an independent ELVA marker (e.g. LAMP1 or RUFY1). For the quantification of ELVA-to-cytoplasm enrichment of GFP and RUFY1-GFP constructs several ELVAs per oocyte were manually segmented as described in the FM4-64FX channel, and the mean GFP intensity inside each segmented ELVA was taken as a readout. Then, the mean intensity of an empty portion of cytoplasm adjacent to each segmented ELVA was measured as the cytoplasmic GFP intensity. The ELVA-to-cytoplasm ratio was calculated for each ELVA for each oocyte and the average ratio taken as the readout for each oocyte. For the quantification of Me4BodipyFL in absence of an independent ELVA marker, ELVAs were segmented manually in the Me4BodipyFL channel as described. The mean intensity of several ELVAs was taken as the readout for each oocyte. In oocytes in which ELVA labelling was too low for correct identification, the mean intensity of several portions of the cytoplasm was taken as the readout. For the quantification of ELVA-to-cytoplasm enrichment of TDP-43, the intensity of TDP-43 inside each ELVA was measured automatically as described. The average cytoplasmic intensity of TDP-43 was measured as follows: first, the LAMP1 channel was averaged with a 10px-radius, then the 3D object counter plugin was run with a threshold low enough to include the whole cytoplasm. Next, the average intensity of the segmented object was measured in the TDP-43 channel. The accuracy of segmentation was evaluated for all oocytes overlaying the segmented object to the raw picture. To calculate the ELVA enrichment ratio, the intensity of TDP-43 inside each ELVA was divided by the average cytoplasmic intensity of the corresponding oocyte. For the quantification of Ubiquitin ELVA-to-cytoplasm ratio in embryos treated with or without BafA1, Ubiquitin intensity inside ELVAs was measured automatically as described. The average cytoplasmic intensity of each embryo was measured taking the mean intensity of several cytoplasmic areas in an average Z-projection of the entire embryo. ELVA-to-cytoplasm ratio was calculated for each ELVA for each embryo, and the average ratio was taken as the readout for each embryo.

Colocalization measurements were performed on individual z-slices. ELVAs were first segmented in FIJI with "Analyze Particle" function as objects larger than 1μm^2 in the reference channel where a known ELVA marker was acquired (e.g., Proteostat or LAMP1), then colocalization with the other channel (e.g. Ubiquitin, FM4-64FX, RUFY1, etc.) was measured with the JACOP plugin. The % overlapped area in the reference channel was taken as readout for each oocyte. For RUFY1 colocalization with ELVAs, the % of the overlapped RUFY1 area was also taken to measure the amount of ELVA-localized RUFY1 respect to the total RUFY1 signal. For RUFY1 colocalization with free lysosomes, lysosomes were first segmented in the LAMP1 channel as objects smaller than 1μm^2, then colocalization with RUFY1 was measured with JACOP as described. For RUFY1 colocalization with both ELVAs and free lysosomes, objects were segmented in the LAMP1 channel without any filter for size, then colocalization with RUFY1 was measured with JACOP as described. Colocalization between RUFY1-GFP compartments and organelle markers in HeLa cells was performed with the JACOP plugin on whole stacks. Pearson's correlation coefficients were taken as readouts.

Quantification of the mean cytoplasmic intensity of ZAR1, G3BP2, LSM14B and 20S was performed on the equatorial section of each oocte/egg/embryo taking the mean intensity of the whole cytoplasm (without nucleus or pronuclei) as readout.

For the quantification of LAMP1 plasma membrane intensity, several lines per oocyte/embryo were drawn across the plasma membrane and the maximal intensity across each line was taken. The average of all measurements was taken as readout for each oocyte.

Quantification of free lysosomes was performed with the particle analyzer tool of FIJI. Particles in the LAMP1 channel with an area comprised between 0.2 and 1μm^2 were counted throughout the whole stacks. For the quantification of the relative amount of the total ELVA area respect to the total lysosomal area, free lysosomes were segmented as described. ELVAs in each slice were segmented in

the RUFY1 channel (most stringent ELVA marker) with the particle analyzer tool as objects with area larger than $1\mu m^2$, then the total lysosomal area was calculated as the total ELVA area plus the total free lysosomal area.

For the quantification of vesicle density in electron microcopy images, the number of autophagosomes and MVBs within each ELVA was counted and divided by the respective ELVA area. Autophagosomes were counted based on the presence of a double membrane, MVBs based on the presence of intraluminal vesicles (ILVs).

All applied statistical tests are indicated in the respective figure legends. p-values are indicated in the respective graphs on top of the samples subjected to comparison. Where applicable and unless otherwise specified data points in the graphs shown represent individual oocytes (the average of all ELVAs in that oocyte). Bars in violin plots represent sample medians. For each experiment, data from multiple independent replicates, each with oocytes from multiple animals randomly distributed among samples, were pooled, and plotted. For comparison between two samples an unpaired t-test with Welch's correction was used. For comparison among multiple samples one-way ANOVA with Šidák correction was used. For comparison among different outcomes a Fischer's exact test was used.

All statistical tests were performed with GraphPad Prism 10 for macOS, GraphPad Software, San Diego, California, USA, www.graphpad.com.

CellPress
OPEN ACCESS

Supplemental figures

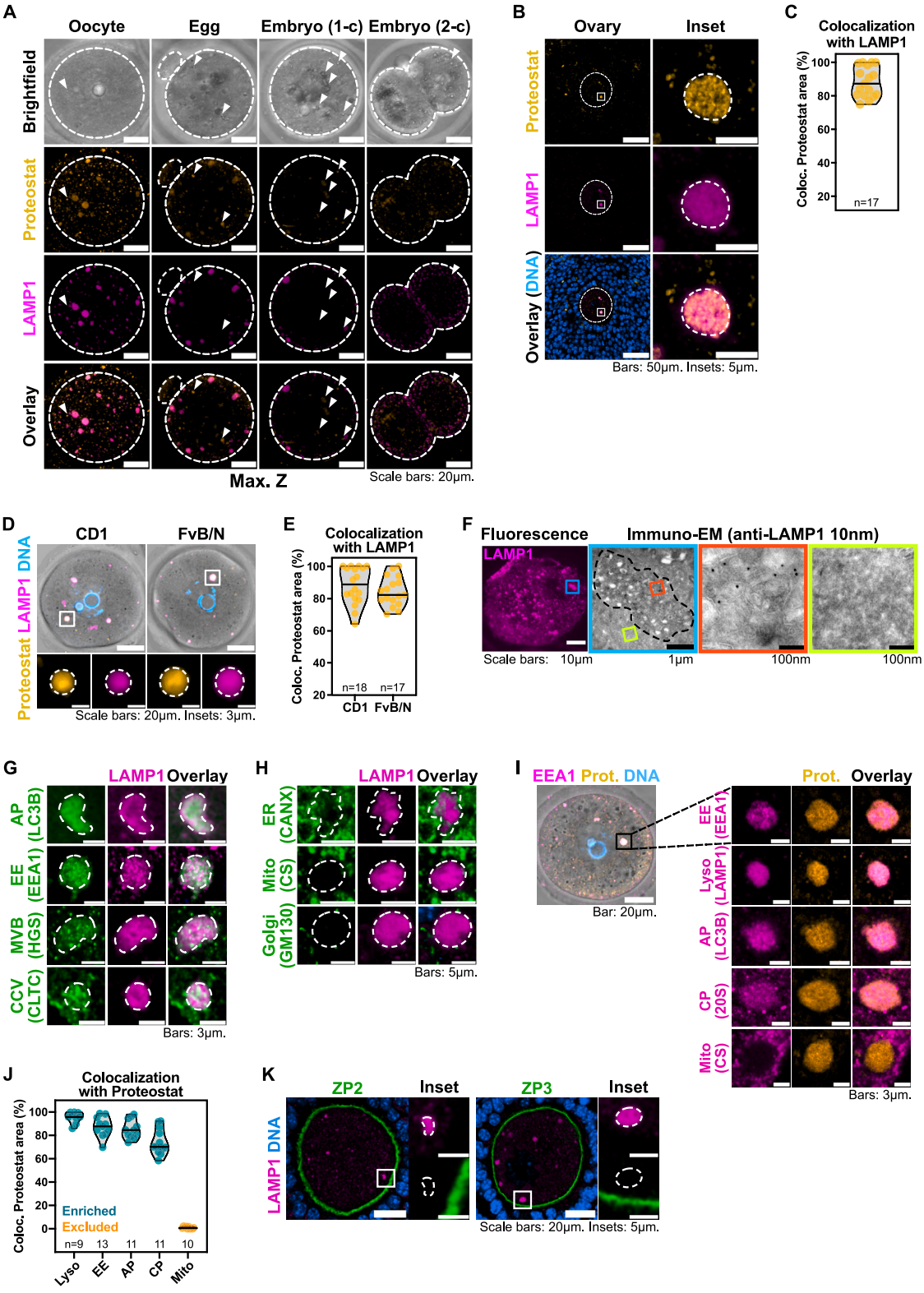

(legend on next page)

Figure S1. ELVAs contain endolysosomal organelles, related to Figure 1

(A) Maximal Z projections of the cells shown in Figure 1A. Notice that Proteostat also tends to label the light-reflective granules visible in brightfield (arrowheads).

(B) Confocal image of a young adult mouse ovarian section labeled with Proteostat and anti-LAMP1.

(C) Quantification of the colocalization between Proteostat and LAMP1 in the experiment shown in (B).

(D) Confocal images of isolated CD1 and FvB/N oocytes labeled with Proteostat and anti-LAMP1.

(E) Quantification of Proteostat colocalization with LAMP1 in the experiment shown in (D).

(F) Immunocorrelative light-electron microscopy (Immuno-CLEM) images of a mouse oocyte section labeled with anti-LAMP1.

(G) Confocal images of ELVAs in mouse oocytes immunolabeled with anti-LAMP1 and the indicated membranous organelles enriched in ELVAs. For each organelle, quantification of the colocalization with ELVAs is shown in Figure 1K. The protein used as a marker of each organelle is indicated in parentheses. AP, autophagosomes; EE, early endosomes; MVB, multivesicular bodies; CCV, Clathrin-coated vesicles.

(H) Confocal images of ELVAs in mouse oocytes immunolabeled with anti-LAMP1 and the indicated membranous organelles excluded from ELVAs. For each organelle, quantification of the colocalization with ELVAs is shown in Figure 1K. The protein used as a marker of each organelle is indicated in parentheses. ER, endoplasmic reticulum; Mito, mitochondria; Golgi, Golgi apparatus.

(I) Confocal images of ELVAs in mouse oocytes labeled with Proteostat and the indicated organelles. The protein used as a marker of each organelle is indicated in parentheses. Lyso, lysosomes; AP, autophagosomes; EE, early endosomes; CP, core proteasomes.

(J) Quantification of Proteostat colocalization with the indicated organelles in the experiment shown in (I). Numbers indicate the number of individual ELVAs from different oocytes quantified per sample.

(K) Confocal images of mouse ovarian sections labeled with anti-LAMP1 and anti-ZP2 (left) or anti-ZP3 (right). Quantification of the colocalization with ELVAs is shown in Figure 1K.

CellPress
OPEN ACCESS

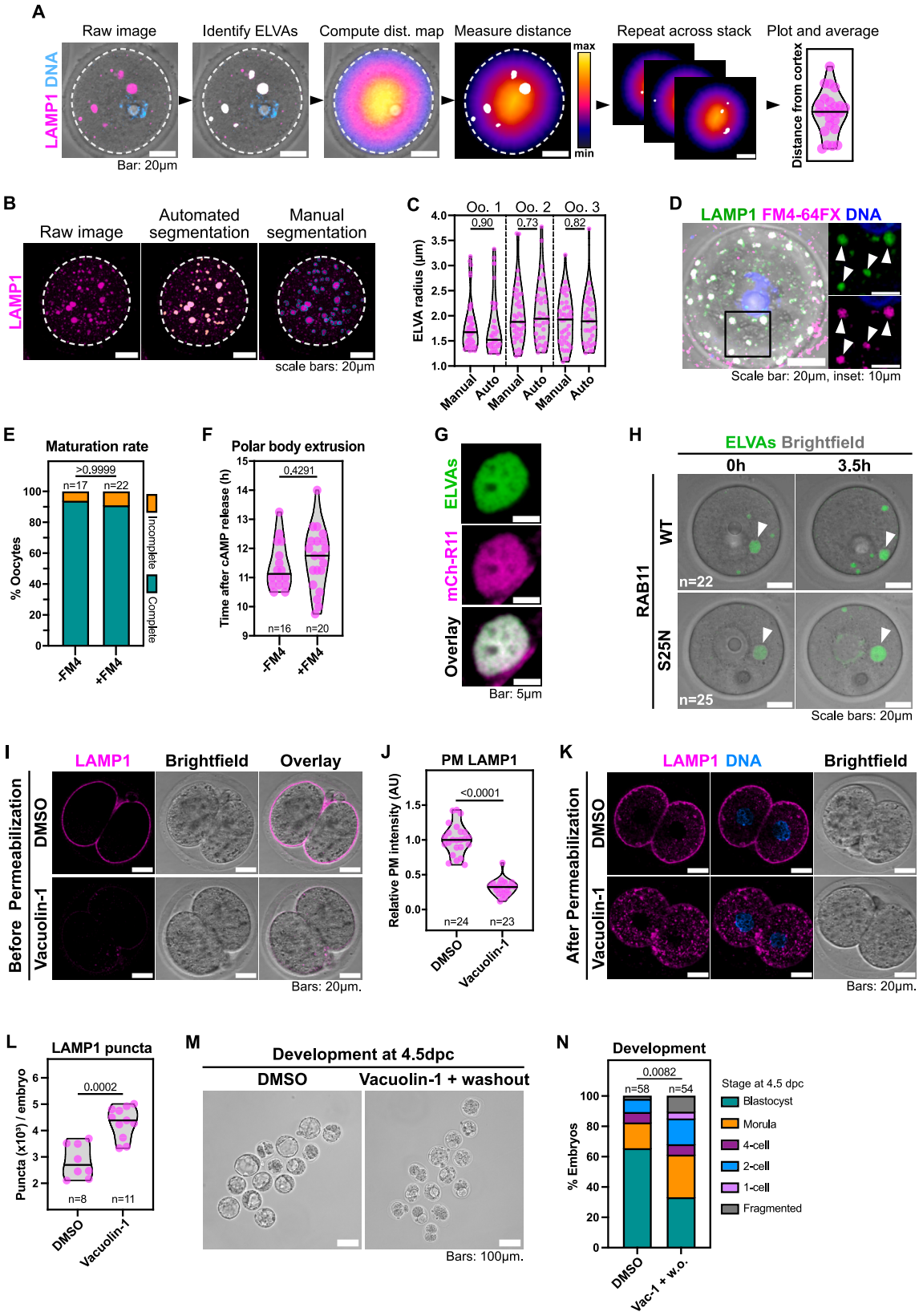

(legend on next page)

Figure S2. ELVAs are dynamic during oocyte maturation, related to Figure 2

(A) Schematic workflow for the quantification of ELVAs and their distance from the cell cortex.

(B and C) Comparison between manual and automated ELVA identification. (B) Left: maximal Z projection of an oocyte immunolabeled with anti-LAMP1. Middle: overlay with automatically identified objects as described in (A). Right: overlay with manually picked objects. (C) Quantification of the radius of individual ELVAs in 3 oocytes by both methods. p values: unpaired t tests with Welch's correction.

(D) Confocal image of a mouse oocyte labeled with FM4-64FX and anti-LAMP1. Maximal Z projection across the equatorial region. Quantification of the co-localization between FM4-64FX and LAMP1 is shown in Figure 1K.

(E) Maturation rate in oocytes labeled with or without FM4-64FX. Maturation was considered complete if a polar body was extruded. p value: Fischer's exact test.

(F) Quantification of the polar body extrusion time in oocytes labeled with or without FM-4-64FX. Times are expressed in hours after the release of the meiotic arrest by db-cAMP washout. p value: unpaired t test with Welch's correction.

(G) Live confocal image of an ELVA in a mouse oocyte injected with mCherry-RAB11A (mCh-R11). ELVAs were detected by co-injection of mClover-LACT-C2[89] in oocytes isolated from FvB/N mice.

(H) ELVA relocation in oocytes injected with RAB11A WT or S25N mutant. ELVAs were detected by co-injection of mClover-LACT-C2[89] in oocytes isolated from FvB/N mice. Note that the FvB/N strain has larger ELVAs. Arrowheads indicate the same ELVAs over time. Live confocal images at the indicated time points after db-cAMP washout.

(I) Confocal images of unpermeabilized 2-cell embryos treated with or without Vacuolin-1 during the first cell division and labeled with anti-LAMP1 1D4B.

(J) Quantification of plasma membrane (PM) LAMP1 intensity. n numbers: individual embryos quantified. p value: unpaired t test with Welch's correction.

(K) Left: confocal images of permeabilized 2-cell embryos treated with or without Vacuolin-1 during the first cell division and labeled with anti-LAMP1 1D4B.

(L) Quantification of intracellular LAMP1 puncta. n numbers: individual embryos quantified. p value: unpaired t test with Welch's correction.

(M) Widefield images of mouse embryos treated with or without Vacuolin-1 during the first cell division, followed by recovery in treatment-free medium for 3 days. Images were taken at 4.5dpc.

(N) Quantification of embryonic development at 4.5dpc. Blastocysts were counted based on the presence of a blastocoel, irrespective of embryo morphology. n numbers: individual embryos quantified. p value: Fischer's exact test.

CellPress
OPEN ACCESS

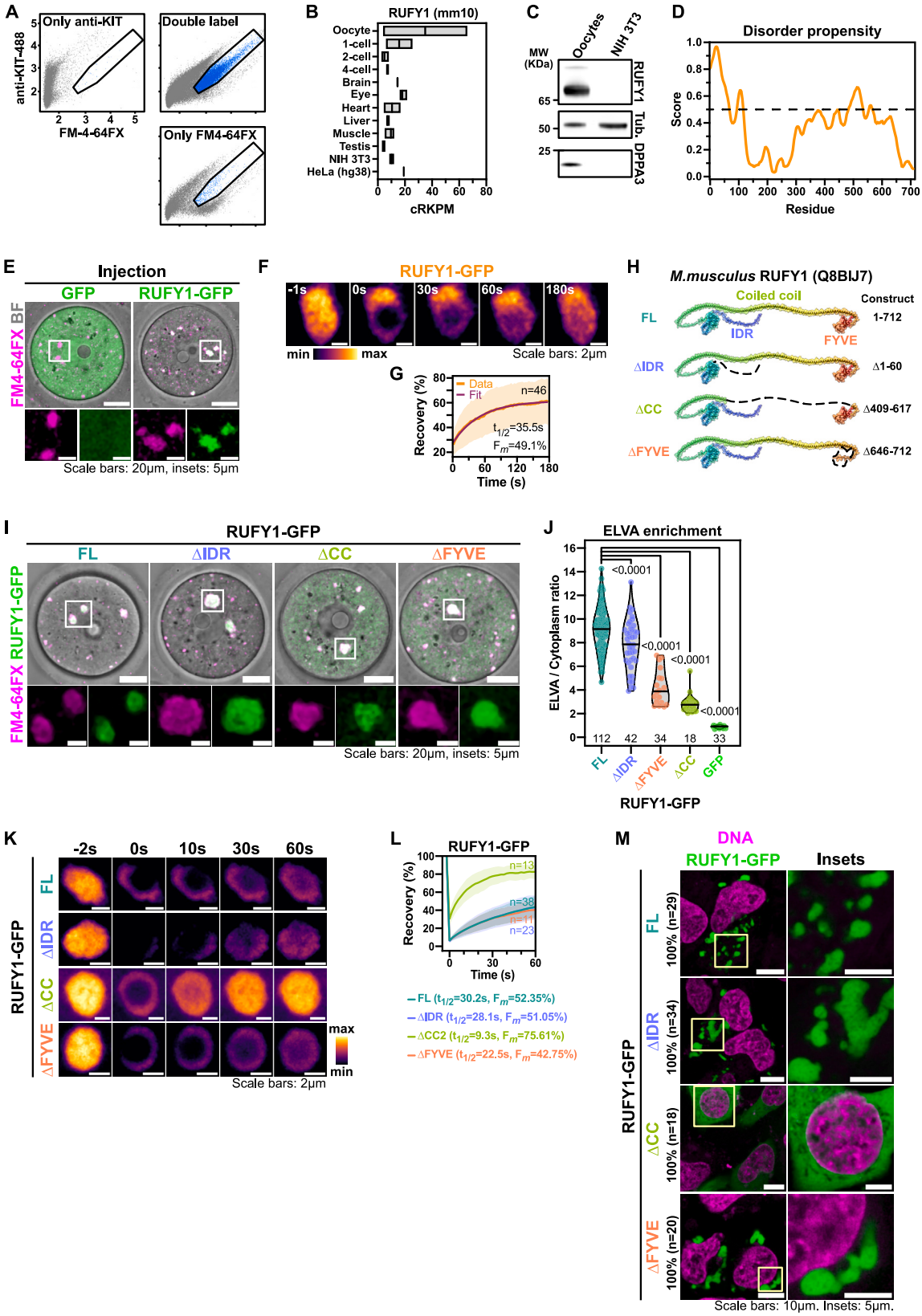

(legend on next page)

Figure S3. RUFY1 as the ELVA matrix protein, related to Figure 3

(A) FAPS plots of oocyte lysates from WT C57BL/6J labeled with anti-KIT-Alexa488 and FM4-64FX or each individual dye alone as a control. Gate is shown as a black box, the sorted population is shown in blue. Log(Intensity) values are displayed on the axes. Axis labels are identical for all the graphs.

(B) RNA expression profiles of mouse RUFY1 across different tissues and cell types. RUFY1 expression in human HeLa cells is also shown. Data were retrieved from VastDB (https://vastdb.crg.eu).[90]

(C) Western blot of mouse oocytes and NIH 3T3 cells probed with the indicated antibodies. DPPA3/Stella was used as a germline marker.[91] Representative image of two independent experiments.

(D) Disorder plot of mouse RUFY1 generated with IUPred3 (long disorder algorithm).[92] The dashed line represents a threshold of 0.5.

(E) Confocal images of mouse oocytes injected with GFP or RUFY1-GFP mRNAs and labeled with FM4-64FX to highlight ELVAs. Quantification of the ELVA enrichment of each protein is provided in (J).

(F) Confocal FRAP recording of a RUFY1-GFP-labeled ELVA in a live mouse oocyte.

(G) Quantification of RUFY1-GFP FRAP recordings. Data were normalized to the pre-bleach intensity (100%). Average and SD are shown. n indicates the number of individual recordings analyzed from multiple oocytes. For the calculation of the recovery half-time ($t_{1/2}$) and the mobile fraction (F_m), data were fitted with a monoexponential curve ($R^2 = 0.9949$).

(H) Schematic representation of RUFY1 protein structure as predicted by AlphaFold.[93] Deleted regions are denoted by dashed lines.

(I) Confocal images of mouse oocytes injected with RUFY1-GFP mutants mRNAs and labeled with FM4-64FX to highlight ELVAs.

(J) Quantification of ELVA enrichment of each GFP-RUFY1 construct from experiments shown in (E) and (I). p values: one-way ANOVA with Šidák correction for multiple comparisons.

(K) Confocal FRAP recordings of ELVAs labeled with RUFY1-GFP mutants in live mouse oocytes.

(L) Quantification of FRAP shown in (K). Data were normalized to the pre-bleach intensity (100%). Averages and SDs are shown. The number of independent recordings quantified per condition is indicated. For the calculation of the recovery half-time ($t_{1/2}$) and the mobile fraction (F_m), each dataset was fitted with a monoexponential curve ($R^2 > 0.99$ for all curves).

(M) Representative confocal images of HeLa cells transfected with RUFY1-GFP mutants.

CellPress
OPEN ACCESS

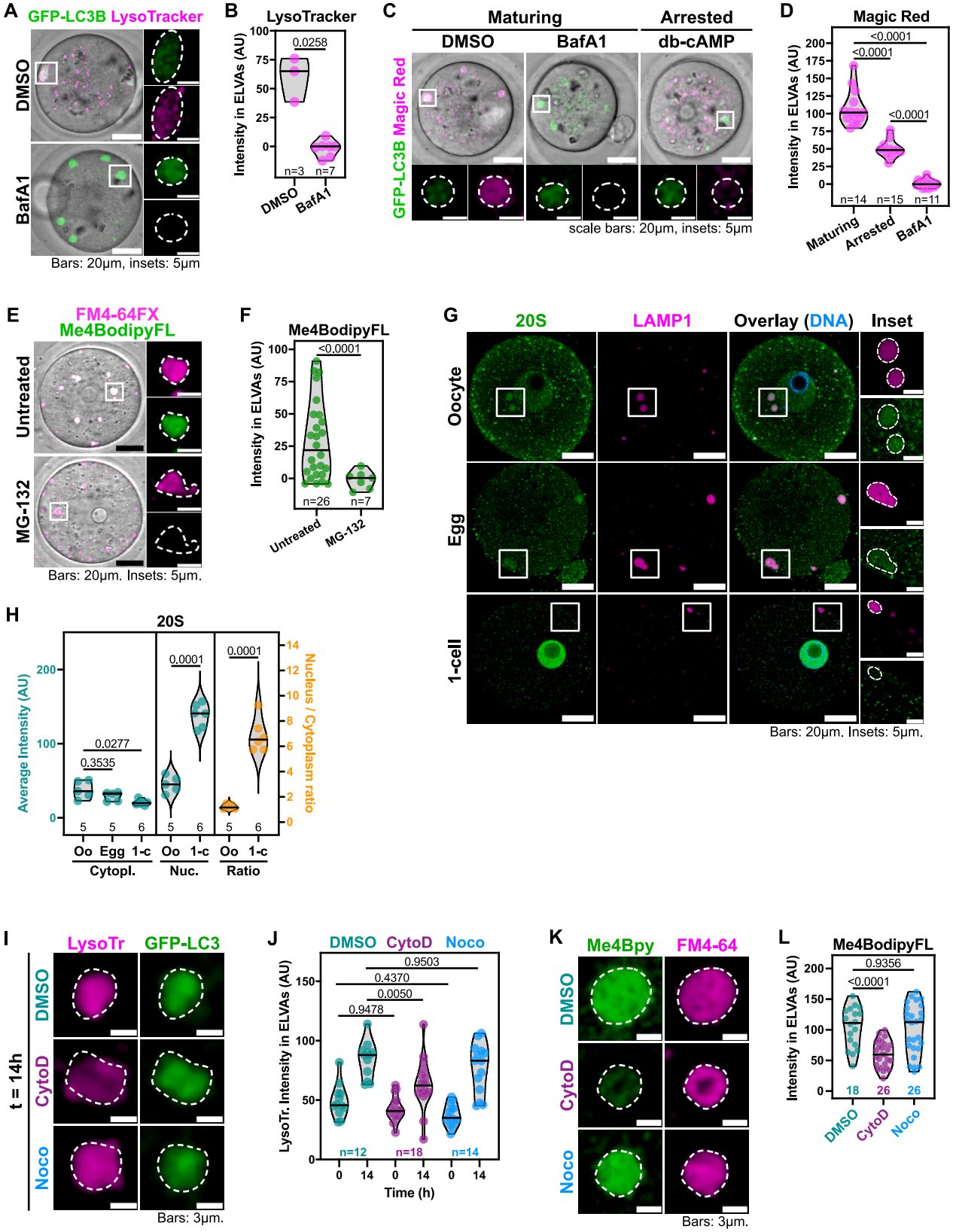

(legend on next page)

Figure S4. The degradation activity of ELVAs is coupled to ELVA relocation, related to Figure 4

(A) Confocal images of GFP-LC3B transgenic oocytes *in vitro* matured in presence or absence of BafA1 followed by labeling with LysoTracker Deep Red. BafA1 treatment still allowed most oocytes to complete maturation.

(B) Quantification of the mean LysoTracker intensity inside ELVAs in the experiment shown in (A). Data were normalized subtracting the median of BafA1 from all samples. p value: unpaired t test with Welch's correction.

(C) Confocal images of GFP-LC3B transgenic oocytes *in vitro* matured in presence of the Magic Red Cathepsin B substrate and of the indicated compounds.

(D) Quantification of the mean Magic Red intensity inside ELVAs in the experiment shown in (C). Data were normalized subtracting the median of BafA1 from all samples. p values: one-way ANOVA with Šidák correction for multiple comparisons.

(E) Confocal images of maturation-competent mouse oocytes treated with or without the proteasomal inhibitor MG-132 and labeled with the proteasome activity probe Me4BodipyFL. ELVAs were labeled with FM4-64FX.

(F) Quantification of the mean Me4BodipyFL intensity inside ELVAs in the experiment shown in (E). Data were normalized subtracting the median of MG-132 from all samples. p values: unpaired t test with Welch's correction.

(G) Representative confocal images of mouse oocytes (SN), eggs, and 1-cell embryos immunolabeled with anti-20S and anti-LAMP1.

(H) Quantification of the average nuclear and cytoplasmic 20S intensity in the experiment shown in (G). p values: Cytoplasm: one-way ANOVA with Šidák correction for multiple comparisons. Nucleus and Ratio: unpaired t tests with Welch's correction.

(I) Live confocal images of ELVAs in transgenic GFP-LC3B oocytes *in vitro* matured in presence of the indicated compounds and labeled with LysoTracker Deep Red.

(J) Quantification of the average (per oocyte) LysoTracker intensity in ELVAs at the indicated time points from db-cAMP washout in the experiment shown in (I). n numbers: individual oocytes quantified. p values: one-way ANOVA with Šidák correction for multiple comparisons.

(K) Live confocal images of ELVAs in mouse oocytes *in vitro* matured in presence of the indicated compounds and labeled with FM-4-64FX and the proteasome activity probe Me4BodipyFL (Me4Bpy).

(L) Quantification of the average (per oocyte) Me4BodipyFL intensity in ELVAs in the experiment shown in (K). n numbers: individual oocytes quantified. p values: one-way ANOVA with Šidák correction for multiple comparisons.

CellPress
OPEN ACCESS

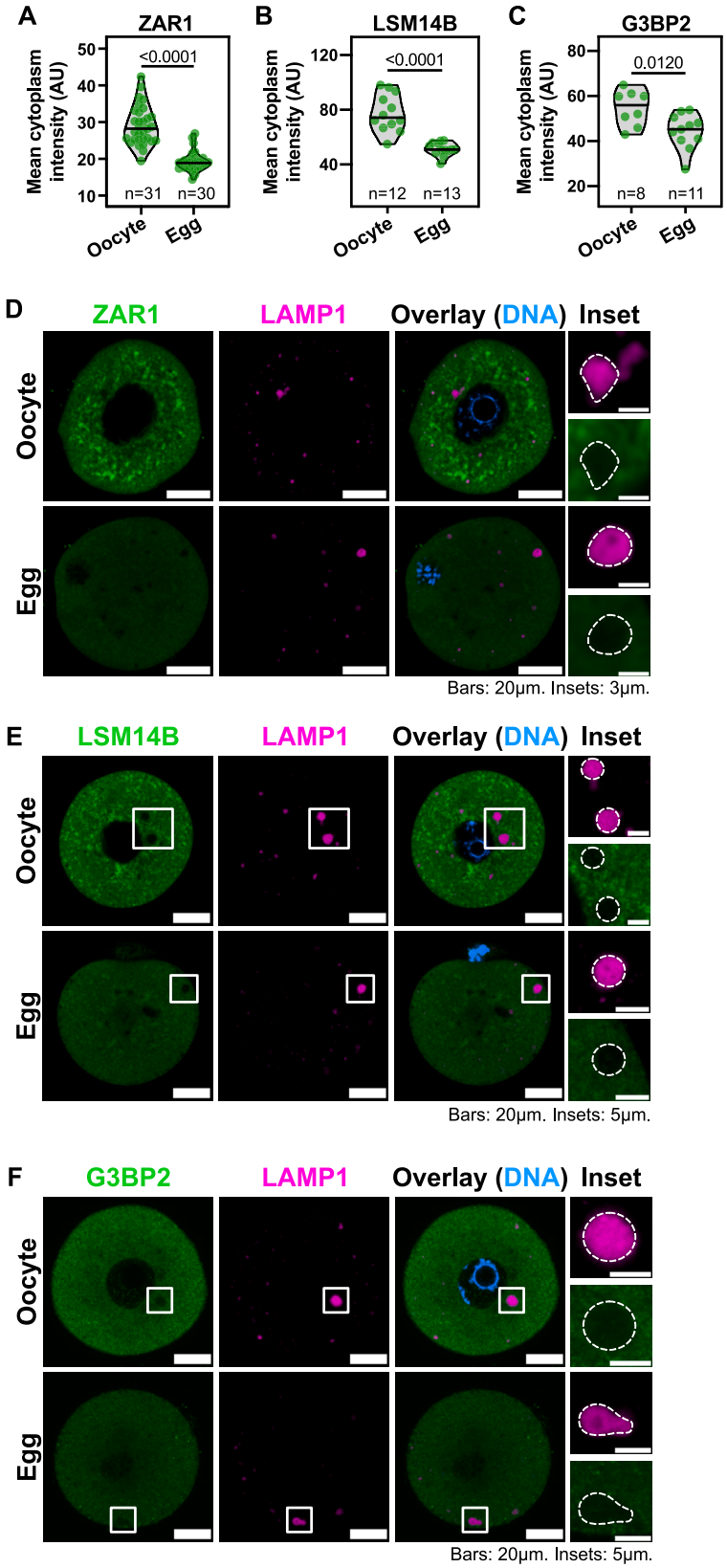

(legend on next page)

Figure S5. ELVAs are a specific degradation route, related to Figure 6

(A–C) Quantification of the mean cytoplasmic intensity of ZAR1 (A), LSM14B (B), and G3BP2 (C) in oocytes and eggs. Representative images of each experiments are shown in (D–F). p values: unpaired t test with Welch's correction.

(D–F) Confocal images of oocytes and eggs immunolabeled anti-LAMP1 and anti-ZAR1 (D), anti-LSM14B (E), or anti-G3BP2 (F).

CellPress
OPEN ACCESS

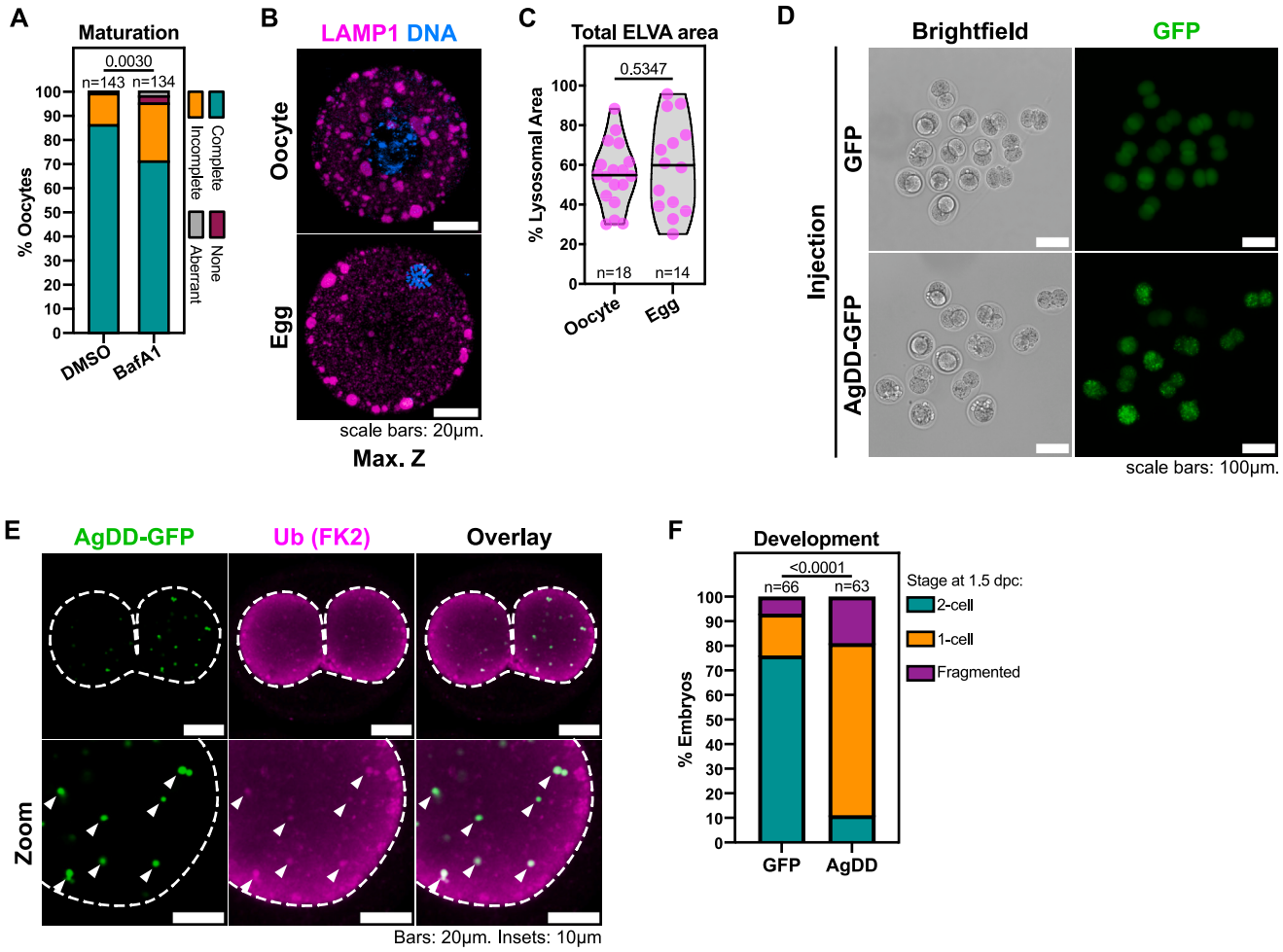

Figure S6. Aggregate degradation is required for oocyte maturation and embryo development, related to Figure 7

(A) Maturation rates of oocytes *in vitro* matured in presence or absence of BafA1. Maturation was considered complete if a polar body was extruded, incomplete if meiosis was resumed (NEBD occurred) but no polar body was extruded, and null if meiosis was not resumed (no NEBD). Oocytes showing blebbing, symmetrical cleavage, or other morphological anomalies were considered aberrant. p value: Fischer's exact test.

(B) Confocal images (maximal Z projections across the equatorial region) of mouse oocyte and egg immunolabeled with anti-LAMP1.

(C) Quantification of the ELVAs area as a fraction of the total lysosomal area in oocytes and eggs. p value: unpaired t test with Welch's correction.

(D) Representative widefield images of embryos injected with GFP or AgDD-GFP mRNA and imaged after the first embryonic cleavage.

(E) Representative confocal images of an embryo injected with AgDD-GFP mRNA and immunolabeled with anti-Ub FK2. Arrowheads indicate ubiquitinated aggregates.

(F) Quantification of development rate in embryos injected with GFP or AgDD-GFP mRNA after one overnight culture. p value: Fischer's exact test.